Computational study of H_2O adsorption and hydrolysis on $(ZnO)_3$ nanoclusters deposited on graphene and graphene oxides

Duwage C. Perera[*] and Jayendran C. Rasaiah[*]

Department of Chemistry, University of Maine, Orono, ME 04469
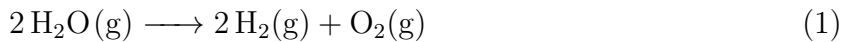
E-mail: charitha.perera@maine.edu; rasaiah@maine.edu

Abstract

Graphene and graphene oxide (GO) based metal oxides could play an important role in photocatalysis using metal oxide catalysts. ZnO is a metal oxide with a 3.37 eV band gap and is a commercially cheaper photocatalyst than titanium oxide in the production of hydrogen (H_2)by splitting water. The π conjugation structure of GO shows greater electron mobility and could enhance the photocatalytic performance of the ZnO catalyst by increasing the electron-hole separation. In this work, we use density functional theory at the B3LYP/DGDZVP2 level to study the impact of adsorbing $(ZnO)_3$ on graphene and GO on the hydration and hydrolysis of water that precedes water splitting to produce H_2 and O_2 in the gas phase. We used 5 different GO models anchoring carboxyl, hydroxyl, and epoxy functional groups on separate layers of graphene. This study also compares the reaction pathway of H_2 and O_2 production from the hydrolyzed $(ZnO)_3$ and GO1-$(ZnO)_3$ in the gas phase using the same level of theory.

Introduction

Ever since Fujishima and Honda first discovered in 1972, the electrochemical photolysis of water in the presence of TiO_2 catalyst to produce H_2 gas has become an active research area to understand the mechanism of photolysis, and to find cheaper substitutes TiO_2 as solutions to current energy problems.[1] Numerous studies show that other nano-scaled metal oxides can also play an important role as photocatalysts in water-splitting reactions 1 to produce H_2, overcoming the cost and challenges of TiO_2.[2–4] However, scaling up H_2 gas production using metal oxides or metal oxide co-catalysts derived from noble metals like Pt, Ru and Rh is a problem due to the high temperatures required for synthesis and related costs. There is also the problem of finding suitable substrates for the photo-catalysts to operate at room temperature.[5]

$$2\,H_2O\,(g) \longrightarrow 2\,H_2(g) + O_2(g) \tag{1}$$

The enthalpy change for water splitting reaction is 116.5 kcal/mol at 298.15 K in the gas phase showing that the reaction is strongly endothermic, and requires $\approx$ two photons of 500 nm wavelength to overcome the enthalpy difference[6] of reaction 1. However, on examining the mechanism of reaction 1 using TiO_2 and different metal oxide catalysts, water splitting is preceded by hydration of the catalyst and hydrolysis of water in exothermic reactions that further lower the enthalpies of reactants thereby increasing the enthalpy for water splitting even more than what is needed for the direct dissociation of two molecules of water to form two molecules of hydrogen and one of oxygen according to the equation 1 in which hydration and hydrolysis are intermediate steps. It is important to study the precursors to water splitting as already done by Fang et al for $(TiO_2)_{n=1\,to\,4}$ and other metal oxides to get a clearer picture of the steps preceding water splitting in the gas phase, using metal oxide catalysts. We have previously studied the $(ZnO)_{n=3}$ nanocatalyst as a substitute for TiO_2 as a catalyst and this paper provides examples of attempts to enhance the catalytic property

of ZnO trimer by deposition on graphene and various synthetic graphene oxides. Graphene shows excellent electron mobility due to its π conjugated structure,[7] which should make it an appropriate substrate material that can accept electrons for exciton separation. However, the hydrophobic property of graphene makes it unsuitable for water-splitting reactions. On the other-hand "suitably functionalized" graphene oxide(GO)s are hydrophilic and have tunable properties and multiple functions that can make them useful substrates for photocatalysts to split water. By "functionalized" we mean different chemical groups attached to graphene to form different GOs.[8–11] Certain metal oxide-decorated carbon materials including GO have also attracted researchers as they exhibit better stability, durability, and electrocatalytic and photocatalytic properties.[12–24]

Since TiO_2 is the most widely studied photocatalyst, systems combining GO and TiO_2 systems have become an important field of study that probes changes in photocatalytic efficiencies of different combinations of GO-TiO_2. The π electrons on suitable GOs can bond with Ti atoms in TiO_2 to fine-tune their window of light absorption. The GO-TiO_2 systems can also form a heterojunction between p-type GO and n-type TiO_2, which operates as a separator of photogenerated electron-hole pairs.[25–27]

ZnO is also a semiconductor with a wide band gap (about 3.37 eV at room temperature)[28] and a wide range of potential applications due to its attractive properties like optical,[29,30] photoelectric[31] and gas sensing.[32] Photocatalytic reduction of carbon dioxide in the presence of ZnO semiconductor powder suspended in a water catalyst has been studied experimentally and it has been reported to be a more efficient photocatalyst than $SrTiO_3$, TiO_2 and WO_3[33–35] in the Fischer-Tropsch synthesis of methanol and methane from CO_2 and H_2O. ZnO nanoclusters are also known to be highly active photocatalysts and are commercially cheaper than TiO_2.[36] Similar to TiO_2, ZnO can also form a p-n heterojunction with a suitable GO for visible light absorption, that could be a better photocatalyst for water splitting[37–40]than some others that are currently in use. Previous computational studies of ZnO($10\bar{1}0$) and

($10\bar{2}0$) sheets in water using QM/MD or neural networks reveal spontaneous partial dissociation of water on the surfaces with proton transfer between adsorbed or bulk water to surface oxygen atom of the ZnO layer.[41–45] Motivated by these reports in the literature,[6] and our own study of bare $(ZnO)_3$ nanoclusters,[46] our ultimate goal is to investigate the mechanism of H_2 and O_2 production via the water splitting reaction 1 using the same $(ZnO)_3$ nanoclusters but now deposited on graphene or suitably functionalized graphene oxides (GOs) anchored on graphene that could be better and cheaper than the TiO_2 catalyst. An essential step, prior to water splitting in the gas phase, is the adsorption of a water molecule on the zinc atom of the photocatalyst followed by hydrolysis that involves simultaneous dissociation of the adsorbed water and proton transfer to a neighboring oxygen atom on the ZnO ring. This hydrolytic process is repeated with a second water molecule that has been studied recently. There are no additional water molecules to solvate each $(ZnO)_3$ nanocluster, as would occur if the lattices were exposed to several water layers or were immersed in an aqueous electrolyte. Following these two steps, the production of H_2 and O_2 occurs through water splitting even in the absence of light.[6,46] It is the mechanisms of these reactions on graphene and on functionalized GOs that are studied in this paper, which are of importance in themselves, and also as a prelude to understanding what occurs when the system is solvated further with more water molecules beyond the bare stoichiometric minimum required 1, which is two for each ZnO trimer and also in the absence of light. This would require modifications to include time to correspond to different light frequencies. To implement the restricted case in the absence of light, we need to be specific about the computational method and the form of the catalyst. We use density functional theory (DFT) with the same basis set and exchange functional that was used in our earlier study of the catalytic activity of bare $(ZnO)_3$ nanoclusters.[46] As before, the triplet state was approximated as the excited singlet state of spin one S_1. We find that the energies of triplet states S_1 are lower than the energies of ground states of spin zero S_0 unlike the energy of the bare $(ZnO)_3$ nanoclusters.[46] We also calculate the energies of absorption and hydrolysis of H_2O on the ZnO trimers in the singlet

and excited triplet states to understand the thermodynamics of adsorption and hydrolysis in each state and construct the corresponding potential energy surfaces (PES) to gain insight into the mechanism of the two processes, and the energy gaps between the singlet and triplet states at different stages of adsorption and hydrolysis. Following this we discuss the reaction pathways for the formation of hydrogen and oxygen on two of the zinc oxide nanocatalysts $(ZnO)_3$ deposited on graphene oxides, GO1, and compare them with what occurs with the bare catalyst that we studied earlier. To the best of our knowledge, this study of different combinations of (ZnO nanocluster-GO) systems has not been reported in the literature.

Computational Method and System Setup

We first studied how $(ZnO)_3$ is absorbed on the graphene sheet in both the parallel and vertical directions followed by adsorption on the GO models. Since determining the exact structure of synthetic GOs is difficult, we modeled the GO surfaces by adding functionality to the optimized graphene sheet using carboxyl, hydroxyl, and epoxy groups similar to the study by Huang and Gubbins.[47] The graphene sheet was computed following the periodic boundary conditions (PBC) explained in the Gaussian tutorial using a benzene ring.[48] A numbered graphene layer of 30 C atom layer is shown in Figure1. We introduced the required functional groups to C atoms 21, 10, 8, and 11 to produce different GO models. We then studied the adsorption of $(ZnO)_3$ on the graphene sheet and on the functional groups of the GO model systems already attached to the graphene sheets. The optimized $(ZnO)_3$ is shown in the figure2.
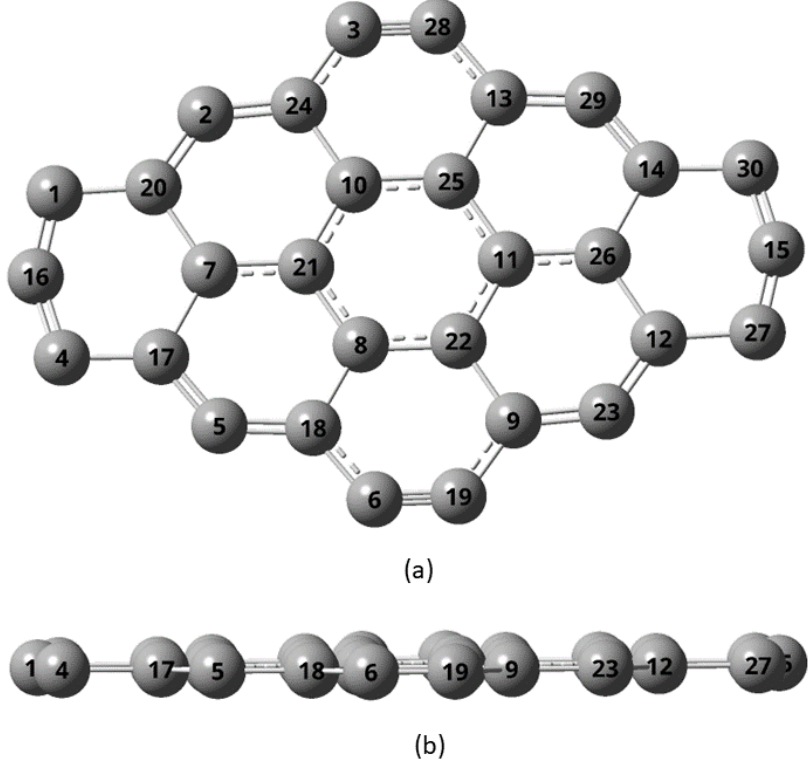
Figure 1: Optimized graphene layer using B3LYP/DGDZVP2 (a) the top view and (b) the side view. C atoms are represented in grey color.
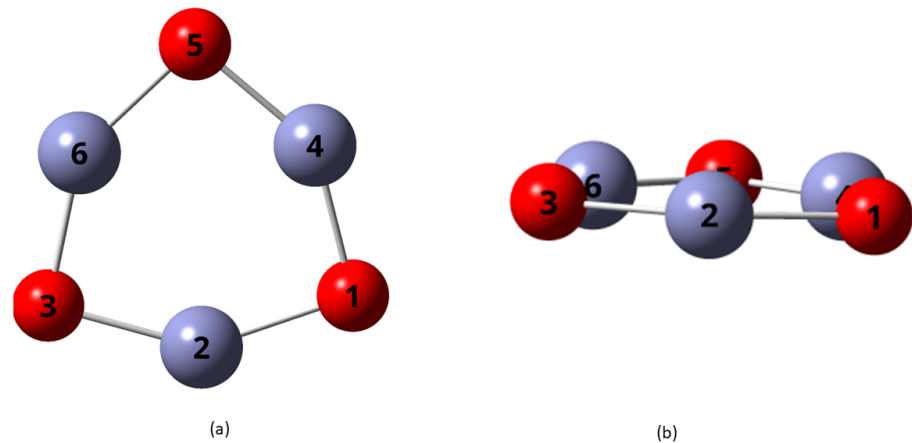
Figure 2: Optimized singlet state ZnO trimer using B3LYP/DGDZVP2. (a) the top view and (b) the side view. Zn and O atoms are represented using light blue and red colors.

All the above structures were optimized using the Becke-Lee-Yang-Parr (B3LYP) exchange-correlation functional and DGDZVP2 Dunning basis set using DFT. The calculation method and specific ZnO cluster system were chosen based on our previous benchmark and basis set studies of small ZnO nanoclusters. We recall that the exchange functional/basis set combination was chosen by us[46] as the best of 30 such combinations of exchange functionals and basis sets and the optimal size of the $(ZnO)_n$ was chosen as n=3 for the best match energy singlet-triplet energy gap with n= 6 as an alternative. We used only n=3 nanocluster and calculated the binding energy of $(ZnO)_3$ on graphene and on the functional groups of each GO model using the same level of theory considering the complexity and the computational time for n=6 clusters. We also calculated and compared the geometric properties, and the free energy and enthalpy changes that accompanied $(ZnO)_3$ adsorption. To each optimized graphene-$(ZnO)_3$ and GO-$(ZnO)_3$ models, we introduced one water molecule to study not only the corresponding binding energy but other properties such as Mulliken charges and changes in the bond length of atoms in $(ZnO)_3$. The hydration and hydrolysis reaction on the selected systems was continued using the second water molecule. We used the hydrolyzed products of the GO1-$(ZnO)_3$ to study the reaction pathway of H_2 and O_2 production.

The same calculation steps were studied on both the singlet (ground state) and excited states (modeled as the triplet state considering the calculation complexity of the excited state using DFT). This provides information on the reorganization and redistribution of charge on the absorbed water molecules before splitting occurs.

All geometry optimization and structural and electronic property calculations were carried out using Gaussian 16 software package[49] and GaussView 6 graphical interface[50] implemented on the University of Maine High-Performance Computer (HPC) resources.

Optimized graphene and graphene oxide models

In this section, we present the results of our studies of graphene and 5 different GO models chosen as substrates for the ZnO photocatalyst. The top and side views of the optimized singlet state graphene structures are shown in Figure 1. The 5 GO models are obtained by attaching carboxyl, hydroxyl, and epoxy functional groups to the graphene layer, as shown in Table 1. The optimized ground state GO models are shown in Figure 3 and the triplet state structures are displayed in the SI document. When a functional group is attached to a carbon atom (chosen as C21) in the graphene sheet in GO models 1-3, the electrons on the neighboring carbon atoms are unpaired to form a double-bond, the (π conjugated system) breaks and the unpaired carbon atoms become saturated with hydrogen atoms. The optimized energies and geometric properties of the GO models in both the singlet and triplet states are tabulated in the SI document.

Table 1: Selected GO models with -COOH, -OH and epoxy functional groups. The C atoms in the GO5 model are the atoms C21 and C8 on which the epoxy group is formed.

C atom attached to the functional group	GO model				
	GO1	GO2	GO3	GO4	GO5
C21		-COOH	-COOH	-OH	-COOH	O
C10						
C8	H					O
C11			H	H	-OH	

In GO1, GO2, and GO4 the functional group -COOH is attached to the C21 atom of graphene with an additional H atom attached to C8 for GO1, and to C11 for GO2. GO4 s similar to GO2 except that an -OH group replaces H at C11 and GO3 is similar to GO2 except that an OH group replaces the -COOH group at C21. In the GO5 model, the functional epoxy O atom straddles C21 and C8 atoms of graphene. All the GO models are twisted and inclined away from the planar graphene structure at the point of attachment to the functional in both ground and triplet states.
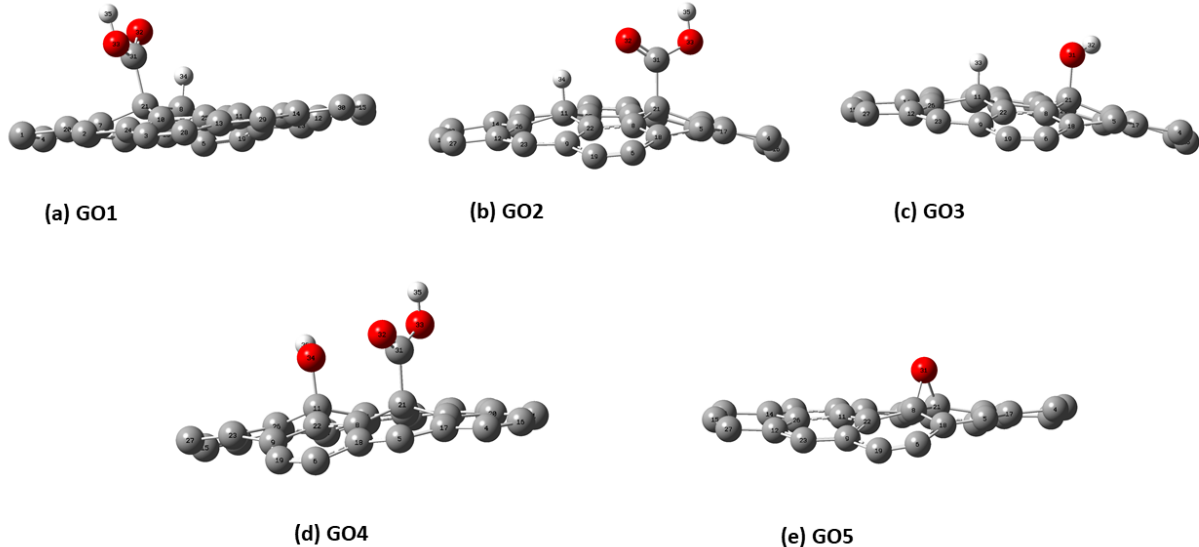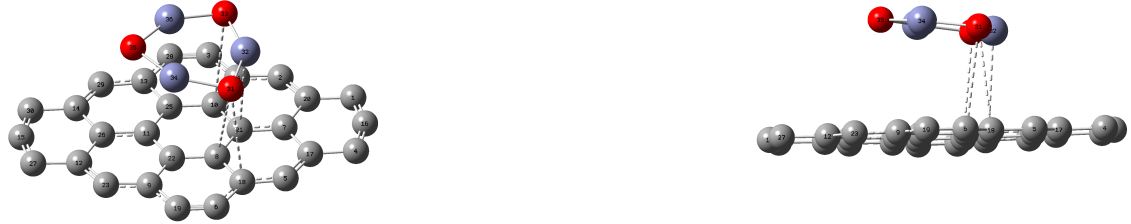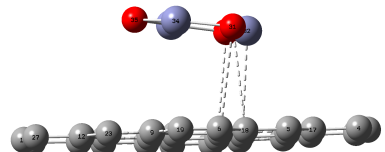
Figure 3: Optimized GO models, (a)GO1, (b)GO2, (c)GO3, (d)GO4 and (e)GO5 using B3LYP/DGDZVP2 level of theory. Grey, red, and light grey color scheme represent the C, O, and H atoms respectively. The top views of all the GO models are in the SI document.

$(ZnO)_3$ adsorption on graphene and graphene oxides GO1-GO5
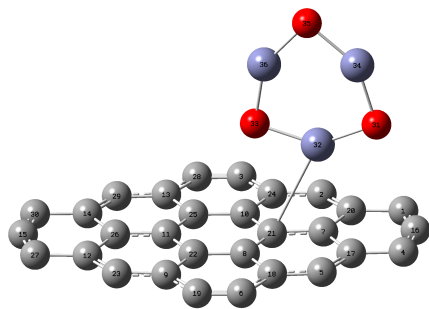
We next attached the optimized $(ZnO)_3$ to graphene and to each GO model before reoptimizing the composite system. The $(ZnO)_3$ cluster is bonded via the Zn2 atom (Figure 2) 2 to graphene in 3 ways in parallel and vertical configurations, and also at the adjacent O atom in the GO models with - COOH functional groups in the cluster. The optimized structures in the singlet state are shown in figure 4, and the triplet state structures are shown in the SI document.
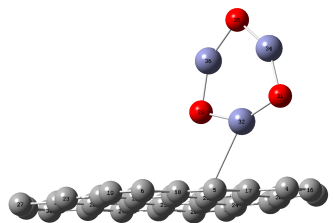
(a) Graphene (P) + (ZnO)$_3$ - top
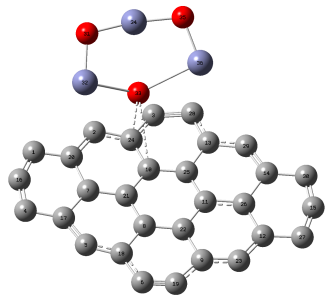
(b) (Graphene (P) + (ZnO)$_3$ - side
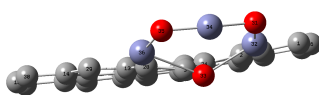
(c) Graphene (V1) + (ZnO)$_3$ - top

(d) Graphene (V1) + (ZnO)$_3$ - side

(e) Graphene (V2) + (ZnO)$_3$ - top

(f) Graphene (V2) + (ZnO)$_3$ - side

Figure 4: Optimized structures of ZnO trimer adsorbed on graphene(a) Top view of (ZnO)$_3$ absorbed parallel to the Graphene, (b) Side view of (ZnO)$_3$ absorbed parallel to the Graphene, (c) Top view of (ZnO)$_3$ absorbed vertically through a Zn atom to the C atom on Graphene, (d) Side view of (ZnO)$_3$ absorbed vertically through a Zn atom to a C atom on Graphene, (e) Top view of (ZnO)$_3$ absorbed vertically through an O atom to two C atoms on Graphene and (f) Side view of (ZnO)$_3$ absorbed vertically through O atom to the Graphene using B3LYP/DGDZVP2 level of theory.
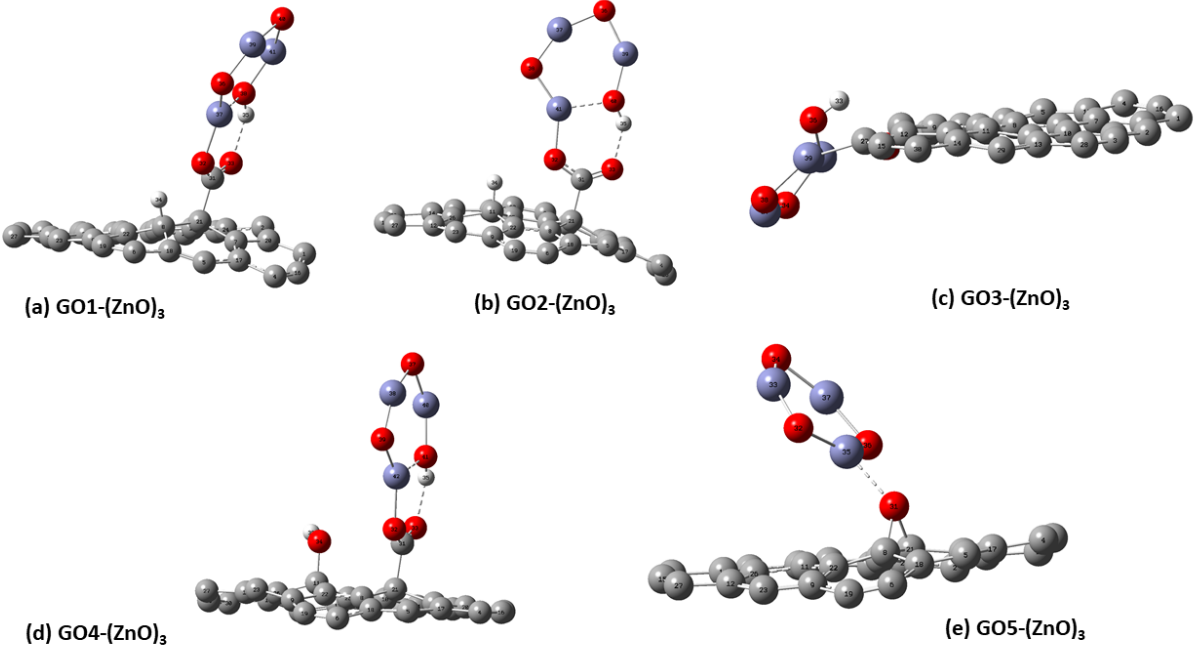
Figure 5: Optimized structures of $(ZnO)_3$ absorbed on (a) GO1, (b) GO2, (c) GO3, (d) GO4, and (e) GO5 respectively using B3LYP/DGDZVP2 level of theory.

$(ZnO)_3$ adsorption energies on graphene and GO models are of interest with respect to their stability as catalytic sites, and were calculated using eq 2 and eq 3 in kcal/mol respectively with the results displayed in the table 2 along with the free energy and enthalpy change of adsorption at 300K.

$$E_{Ad1} = E_{Tot} - (E_{ZnO3} + E_{Graphene}) \tag{2}$$

$$E_{Ad2} = E_{Tot} - (E_{ZnO3} + E_{GO}) \tag{3}$$

In equation 2, E_{Tot} is the energy of the system after adsorbing $(ZnO)_3$ on graphene, and in equation 3, it is the energy of the system after adsorbing $(ZnO)_3$ on a GO model. The energy and free energy of adsorption at 300K are more negative in the triplet than in the single states, and more negative for the GO models than for graphene, which is reflected in the more negative total energies of the triple states than the singlet states. Adsorption is

11

Table 2: $(ZnO)_3$ cluster adsorption energies on each graphene and GO model and, ΔG and ΔH values for the adsorption

System B3LYP/DGDZVP2	E_{Ad} in kcal/mol		ΔG in kcal/mol		ΔH in kcal/mol	
	Singlet	Triplet	Singlet	Triplet	Singlet	Triplet
$(ZnO)_3$ -Graphene - vertical 1	-6.40	-89.09	-12.39	-93.83	-6.02	-86.74
$(ZnO)_3$ -Graphene - vertical 2	-142.68	-	-138.94	-	-139.10	-
$(ZnO)_3$ -Graphene - parallel	-3.04	-257.70	-8.25	-251.90	-3.29	-251.21
$(ZnO)_3$- GO1	-50.46	-108.35	-53.92	-111.87	-49.68	-107.26
$(ZnO)_3$- GO2	-49.86	-108.01	-53.75	-111.85	-49.21	-106.74
$(ZnO)_3$- GO3	-	-	-	-	-	-
$(ZnO)_3$- GO4	-51.78	-108.28	-55.33	-111.56	-51.10	-107.06
$(ZnO)_3$- GO5	-12.83	-100.55	-17.12	-101.89	-11.65	-97.08

driven by a negative enthalpy change and a small negative entropy change. Adsorption of the ZnO trimer parallel to graphene is less favorable in the singlet state that in the triplet state. The magnitudes of the energy and free energy of adsorption (49 -112kcal/mol), for the GO models, except GO5 and graphene(vertical1 and parallel) in the singlet states, suggest chemical rather than physical adsorption corresponding to chemical bonding. Interestingly, the triplet structures have lower energies than the corresponding singlet states, unlike the bare ZnO trimer where the order is reversed.

Table 3: Bond lengths between atoms on $(ZnO)_3$ before and after absorption on graphene and GO systems. Triplet state lengths are shown in parenthesis.

Model	Bond Length in Å					
	1O-2Zn	2Zn-3O	3O-6Zn	6Zn-5O	5O-4Zn	4Zn-1O
$(ZnO)_3$	1.833(1.950)	1.833(1.950)	1.833(1.833)	1.833(1.829)	1.833(1.829)	1.833(1.833)
$(ZnO)_3$-Graphene-Vertical 1	1.847(1.851)	1.859(1.851)	1.825(1.824)	1.829(1.832)	1.834(1.832)	1.823(1.824)
$(ZnO)_3$-Graphene- Parallel	1.833	1.833	1.834	1.833	1.836	1.835
$(ZnO)_3$-GO1	1.834(1.836)	2.073(2.096)	1.837(1.831)	1.802(1.803)	1.840(1.840)	1.795(1.792)
$(ZnO)_3$-GO2	1.836(1.838)	2.074(2.087)	1.835(1.831)	1.802(1.803)	1.839(1.840)	1.794(1.792)
$(ZnO)_3$-GO4	1.832(1.837)	2.085(2.098)	1.833(1.829)	1.802(1.804)	1.840(1.840)	1.793(1.792)
$(ZnO)_3$-GO5	1.857(1.876)	1.870(1.868)	1.818(1.811)	1.830(1.834)	1.832(1.830)	1.818(1.813)

The adsorption of the $(ZnO)_3$ on graphene and on GO models is accompanied by charge distribution on the atoms and changes in bond lengths between atoms of the ZnO nanocluster.

The bond lengths between the atoms on $(ZnO)_3$ are shown in table 3. In the bare $(ZnO)_3$ nanocluster the Zn-O bond length is 1.833 Åin the singlet state. All the triplet state bond lengths are greater or nearly the same as the singlet states values. When $(ZnO)_3$ adsorbed parallel to graphene the Zn-O bond lengths in the trimer have not changed significantly. The slight increment occurs only where the ring structure binds to the graphene in the singlet state, which is in 1O-4Zn, 4Zn-5O, and 3O-6Zn bond lengths. When binding vertically on the graphene sheet, and on the GO models via the 2Zn atom, the 1O-4Zn, 4Zn-5O, and 3O-6Zn bond lengths of the trimer in the singlet state have increased.

Table 4: Bond lengths between atoms on $(ZnO)_3$ and atoms on graphene or GO systems in the singlet and triplet states after adsorption.

Model	Bond Length in A		
	Bond	Singlet	Triplet
$(ZnO)_3$-GV1	2Zn-C	2.954	2.741
$(ZnO)_3$-GV2	5O-C	2.369	N/A
$(ZnO)_3$-GP	4Zn-C	3.302	N/A
	5O-C	3.409	N/A
$(ZnO)_3$-GO1	2Zn-O	1.923	1.908
	3O-H	0.984	0.988
$(ZnO)_3$-GO2	2Zn-O	1.917	1.909
	3O-H	0.985	0.990
$(ZnO)_3$-GO4	2Zn-O	1.915	1.907
	3O-H	0.983	0.991
$(ZnO)_3$-GO5	2Zn-O	2.183	2.152

The bond lengths between the Zn and O atoms in the $(ZnO)_3$ and the atoms in the graphene and GO models calculated using B3LYP/DGDZVP2 are shown in the table4. The triplet state 2Zn- C(graphene) and 2Zn-O(GO) bond lengths are smaller than the singlet state bond. This shows the appearance of stronger bonds on the triplet state with lower optimized energies in the triplet state compared to the singlet state. The 3O($(ZnO)_3$)-H(GO) bond length is larger in the triplet state than in the singlet state.

The Mulliken charges on atoms of the $(ZnO)_3$ cluster before and after adsorption on graphene, graphene oxide, and water are shown in the table 5. Although not unique, the Mulliken

charges on the atoms provide a qualitative understanding of the changes in charge density before and after the absorption on graphene and GO, models,

Table 5: Mulliken charges of atoms in $(ZnO)_3$ without and with H_2O before and after adsorb on the graphene and GO models in the singlet state.

System	Mulliken Charges					
B3LYP/DGDZVP2	1O	2Zn	3O	4Zn	5O	6Zn
$(ZnO)_3$	-0.757	0.757	-0.757	0.757	-0.757	0.757
$(ZnO)_3 + H_2O$	-0.886	0.779	-0.764	0.738	-0.778	0.750
$(ZnO)_3$ -Graphene-parallel	-0.745	0.736	-0.744	0.746	-0.741	0.747
$(ZnO)_3$ -Graphene-vertical	-0.767	0.665	-0.811	0.758	-0.753	0.766
$(ZnO)_3$ -Graphene + H_2O- vertical 1-pathway 1	-0.776	0.702	-0.912	0.759	-0.773	0.752
$(ZnO)_3$ -Graphene + H_2O - vertical 1-pathway 2	-0.766	0.680	-0.828	0.783	-0.878	0.753
$(ZnO)_3$- GO1	-0.753	0.786	-0.715	0.767	-0.724	0.835
$(ZnO)_3$- GO1 + H_2O-pathway 1	-0.876	0.815	-0.701	0.743	-0.745	0.814
$(ZnO)_3$- GO1 + H_2O -pathway 2	-0.768	0.775	-0.737	0.767	-0.779	0.801
$(ZnO)_3$- GO2	-0.725	0.767	-0.759	0.829	-0.711	0.774
$(ZnO)_3$- GO2+ H_2O -pathway 1	-0.746	0.745	-0.888	0.813	-0.698	0.807
$(ZnO)_3$- GO2+ H_2O -pathway2	-0.783	0.767	-0.773	0.797	-0.731	0.763
$(ZnO)_3$- GO4	-0.726	0.766	-0.751	0.833	-0.721	0.780
$(ZnO)_3$- GO4+ H_2O -pathway 1	-0.784	0.766	-0.764	0.800	-0.734	0.768
$(ZnO)_3$- GO4+ H_2O -pathway 2	-0.746	0.744	-0.880	0.814	-0.704	0.809
$(ZnO)_3$- GO5	-0.778	0.745	-0.755	0.711	-0.804	0.753
$(ZnO)_3$- GO5 + H_2O-pathway 1	-0.901	0.738	-0.773	0.766	-0.820	0.755
$(ZnO)_3$- GO5+ H_2O -pathway 2	-0.814	0.722	-0.808	0.721	-0.779	0.738

Polarization follows from a small rearrangement of charge when the oxygen atom of a water molecule is adsorbed on the 2Zn atom of the ZnO trimer. The partial positive charge on 2Zn is increased slightly while the magnitude of the negative charge of the adjacent 1O atom is increased. Exceptions are graphene and GO5 structure where the charge on 2Zn decreases, after water adsorption accompanied by a larger decrease in the negative charge of the 1O oxygen atom in GO5 than in other systems. This could be a reflection of the epoxy structure of GO5.Likewise the densities of state and band gaps provide information on how electron excitation of the $(ZnO)_3$ catalytic center is modulated by graphene and GO model substrates. Our calculations using the using B3LYP/DGDZVP2 level of DFT theory are displayed in Figure 6.

h
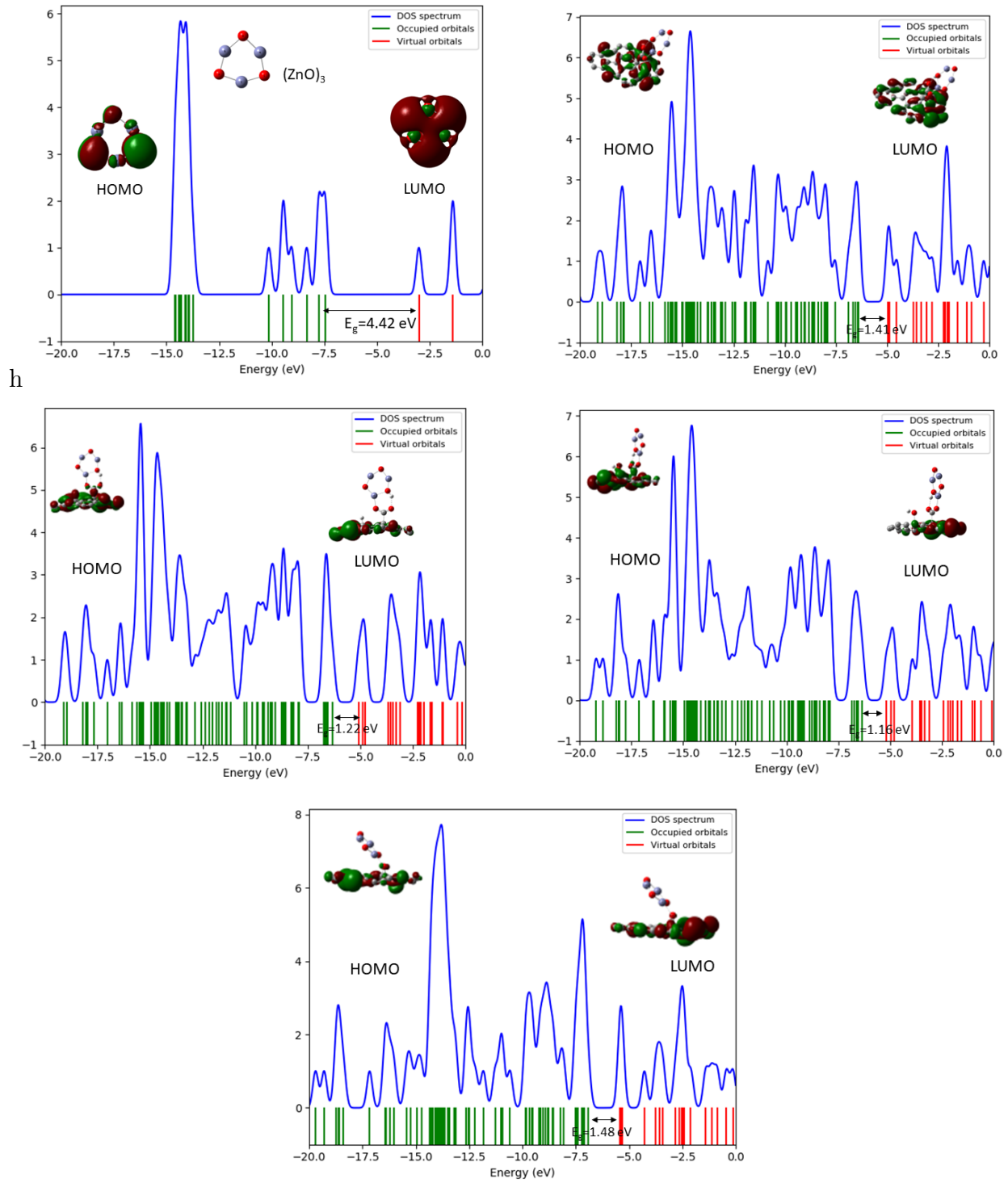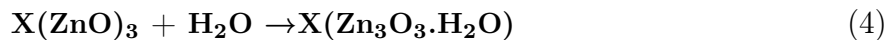
Figure 6: Calculated density of states using GaussSum for (a)$(ZnO)_3$, and $(ZnO)_3$ adsorbed on (b) GO model 1; GO1, (c) GO model 2; GO2, (d) GO model 4; GO4, and (e) GO model 5; GO5.

Results and Discussion
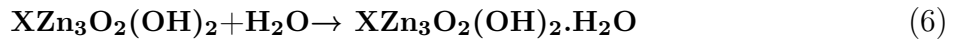
We next discuss successive steps of adsorption and hydrolysis of two water molecules that occur prior to water splitting. [46] The first adsorption step

$$\mathbf{X(ZnO)_3 + H_2O \rightarrow X(Zn_3O_3.H_2O)} \tag{4}$$

is followed by hydrolysis

$$\mathbf{X(Zn_3O_3.H_2O) \rightarrow XZn_3O_2(OH)_2} \tag{5}$$
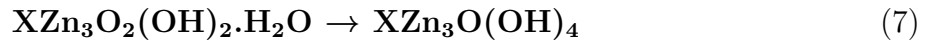
Likewise the adsorption of a second water molecule

$$\mathbf{XZn_3O_2(OH)_2 + H_2O \rightarrow XZn_3O_2(OH)_2.H_2O} \tag{6}$$

is followed by hydrolysis

$$\mathbf{XZn_3O_2(OH)_2.H_2O \rightarrow XZn_3O(OH)_4} \tag{7}$$

where X is either graphene or a GO system. If X is removed what remains is the bare $(ZnO)_3$ nanocluster and its hydrated and hydrolyzed products discussed in our earlier study. [46]

H_2O absorption on catalytic sites

The adsorption of a water molecule occurs directly on a Zn atom of the ZnO trimer already adsorbed on graphene or on the ZnO trimer bonded to a functional group in GO. This is of interest as it is the catalytic site at which hydrolysis begins before water splitting. The negative oxygen atom of a water molecule is adsorbed onto a positively charged Zn atom of the ZnO trimer followed by hydrolytic dissociation and proton transfer of a hydrogen atom

to an oxygen atom adjacent to zinc.
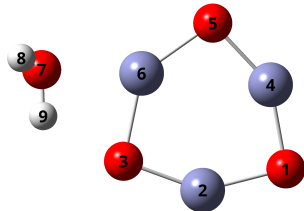
Figure 7: Optimized structures of H_2O absorbed on $(ZnO)_3$ using B3LYP/DGDZVP2 level of theory. Zn, O, and H atoms are represented using the blue, red, and grey colors respectively.

(a) Graphene-$(ZnO)_3$-H_2O-V1-top

(b) Graphene-$(ZnO)_3$-H_2O-V1-side

(c) Graphene-$(ZnO)_3$-H_2O-V2-top

(d) Graphene-$(ZnO)_3$-H_2O-V2-side
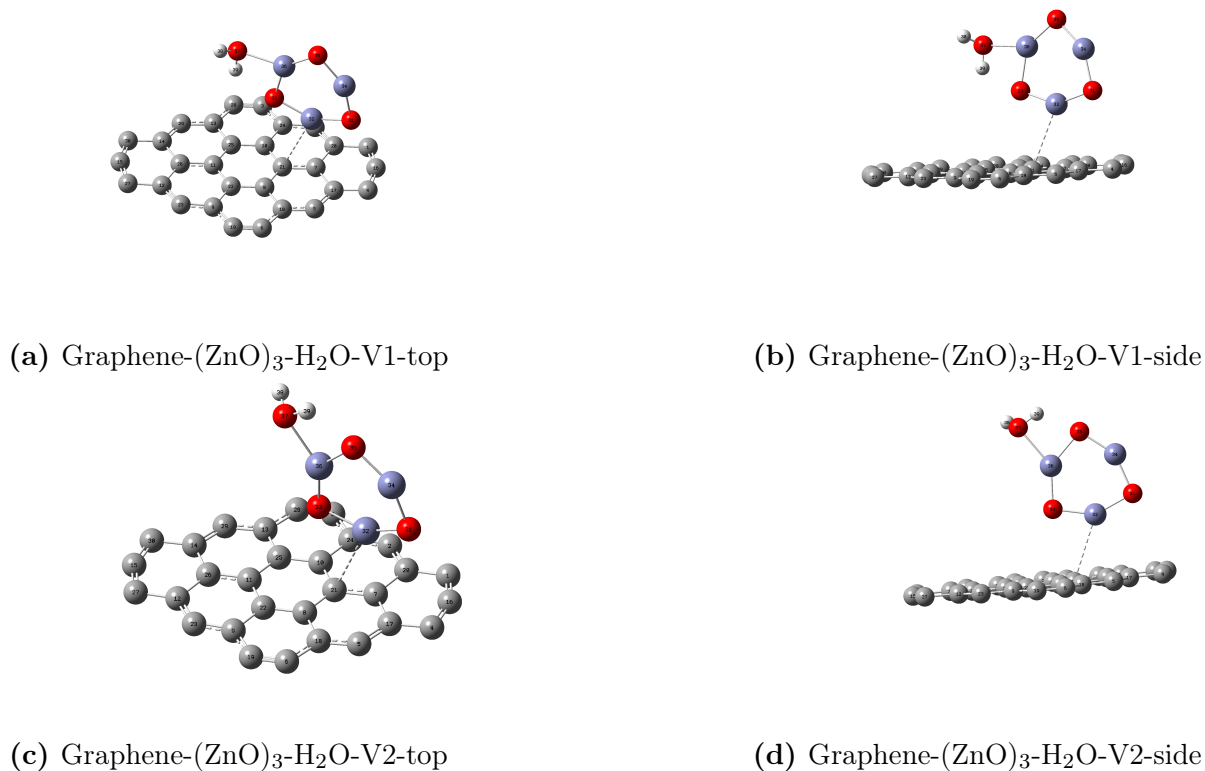
Figure 8: Optimized structures of H_2O adsorption on Graphene-$(ZnO)3$ system - vertical 1 (Zn-C bond) (a)pathway 1 top view, (b)pathway 1 side view, (c) pathway 2 top view, and (d) pathway 2 side view calculated using B3LYP/DGDZVP2.

Figure 7 shows the adsorption of a water molecule on the $(ZnO)_3$ catalyst in the singlet state. A detailed study on the adsorption and hydrolysis reaction of this system has been done in our previous study.[46] Figure 8 shows the water molecule adsorption on graphene-$(ZnO)_3$

model, where V1 and V2 represented the two different vertical adsorptions of $(ZnO)_3$ on the graphene on the singlet state.

(a) GO1-(ZnO)$_3$-H$_2$O-1a

(b) GO1-(ZnO)$_3$-H$_2$O-2a

(c) GO2-(ZnO)$_3$-H$_2$O-1a

(d) GO2-(ZnO)$_3$-H$_2$O-2a

(e) GO4-(ZnO)$_3$-H$_2$O-1a

(f) GO4-(ZnO)$_3$-H$_2$O-2a

(g) GO5-(ZnO)$_3$-H$_2$O-1a

(h) GO5-(ZnO)$_3$-H$_2$O-2a
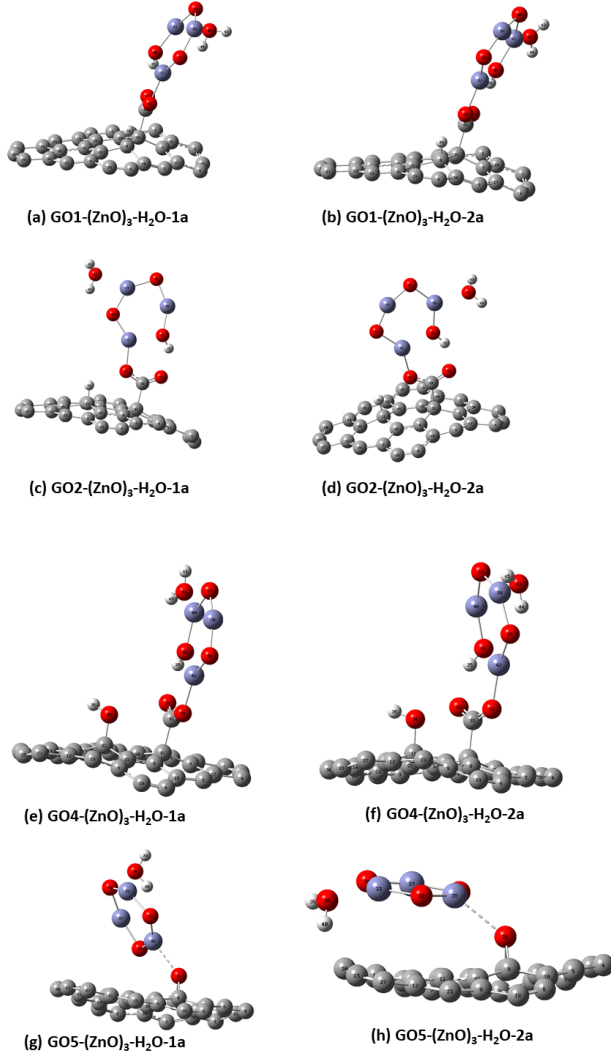
Figure 9: Optimized structures of H_2O absorption on (a) GO1-$(ZnO)_3$:Pathway1, (b) GO1-$(ZnO)_3$:Pathway2, (c) GO2-$(ZnO)_3$:Pathway1, (d) GO2-$(ZnO)_3$:Pathway2, (e) GO4-$(ZnO)_3$:Pathway1, (f) GO4-$(ZnO)_3$:Pathway2, (g) GO5-$(ZnO)_3$:Pathway1 and (h) GO5-$(ZnO)_3$:Pathway2 calculated using B3LYP/DGDZVP2 level of theory

Figure 9 shows the optimized structures of H_2 adsorption on $(ZnO)_3$ anchored on GO 1, 2, 4 and 5 models. Each model goes through two different hydration pathways. Water molecule adsorption energies in kcal/mol on a ZnO trimer already deposited on graphene

are calculated from

$$E_{Ad4} = E_{Tot} - (E_{Graphene} + E_{ZnO} + E_{Water}) \qquad (8)$$

and the corresponding energies of adsorption of ZnO trimer attached to a functional group on GO are calculated likewise from

$$E_{Ad5} = E_{Tot} - (E_{GO} + E_{ZnO} + E_{Water}) \qquad (9)$$

In equation (5), E_{Tot} is the energy of the system after adsorbing $(ZnO)_3$ on graphene, and in equation (5), it is the energy of the system after the water molecule is adsorbed on $(ZnO)_3$ bonded to the functional group of the GO model. The thermodynamic (ΔG) and (ΔH) values were calculated in each reaction using the following relationships,

$$\Delta G_{reaction} = G_{Products} - G_{Reactants} \qquad (10)$$

$$\Delta H_{reaction} = H_{Products} - H_{Reactants} \qquad (11)$$

Our results are presented in table 6 together with the HOMO-LUMO gap in the singlet state before and after the addition of one water molecule. Again the energies and free energies of adsorption in the triplet state are more negative than in the singlet state which is reflected in the total energy. Hydration is driven by the enthalpy change modulated by a substantial negative entropy contribution. Since DFT is a ground state theory, calculations of the HOMP-LUMO gaps using this theory are subject to errors that are well known, but our calculations using DFT should depict the trends in the HOMO-LUMO gap when the zinc oxide trimer is adsorbed on graphene or the functional groups of the GO models. The gap is substantially reduced from 4.42ev for the bare Zinc oxide trimer to 1.21,1.16 and 1.48 eV respectively for the Zinc oxide trimer on GO2, GO3, and GO5, suggesting that GO models will be sensitive to light and electron promotion in the visible region.

Table 6: Water molecule adsorption energy and ΔG, ΔH values in both singlet and triplet states and $\Delta E_{\text{HOMO-LUMO}}$ in the singlet state. The HOMO-LUMO difference of the models before water adsorption is shown within parenthesis.

System B3LYP/DGDZVP2	E_{Ad} in kcal/mol Singlet	Triplet	ΔG in kcal/mol Singlet	Triplet	ΔH in kcal/mol Singlet	Triplet	$\Delta E_{\text{HOMO-LUMO}}$ in eV
$(ZnO)_3 + H_2O$	-19.19	-18.95	-8.24	-8.14	-17.55	-17.26	4.65 (4.42)
$(ZnO)_3$ -Graphene + H_2O- vertical 1-pathway 1	-23.78	-107.68	-4.62	-83.80	-21.68	-103.29	1.46 (1.45)
$(ZnO)_3$ -Graphene + H_2O - vertical 1-pathway 2	-25.10	-107.73	-5.60	-84.19	-23.01	-103.55	1.45 (1.45)
$(ZnO)_3$- GO1 + H_2O-pathway 1	-70.29	-124.75	-48.45	-100.99	-67.79	-122.76	1.42 (1.41)
(ZnO)- GO1 + H_2O -pathway 2	-74.44	-127.64	-53.15	-104.17	-71.93	-125.17	1.44 (1.41)
$(ZnO)_3$- GO2+ H_2O -pathway 1	-69.44	-127.17	-47.94	-102.03	-67.13	-124.24	1.20 (1.22)
$(ZnO)_3$- GO2+ H_2O -pathway2	-73.33	-130.34	-52.51	-106.27	-70.99	-127.41	1.19 (1.22)
$(ZnO)_3$- GO4+ H_2O -pathway 1	-74.77	-118.83	-53.69	-95.85	-71.76	-115.38	1.12 (1.16)
$(ZnO)_3$- GO4+ H_2O -pathway 2	-71.76	-115.38	-49.43	-91.81	-69.36	-113.67	1.14 (1.16)
$(ZnO)_3$- GO5 + H_2O-pathway 1	-30.63	-113.61	-9.25	-87.58	-27.85	-109.07	1.49 (1.48)
$(ZnO)_3$- GO5+ H_2O -pathway 2	-32.70	-116.89	-8.68	-87.57	-30.05	-112.33	1.22 (1.48)

Hydrolysis of Water at catalytic sites of ZnO trimers

In this section, we discuss the mechanistic pathways and potential energy diagrams for hydrolysis in detail. The mechanism is determined using the intrinsic reaction coordinate (IRC) method in the forward and reverse directions suggested by Fukui et al.[?] The hydrolysis of water molecules absorbed on free ZnO trimers, and on the same trimers adsorbed on graphene and the functional groups of the four graphene oxides GO1, GO2, GO4, and GO5 generally involve partial dissociation of the water and proton transfer to a neighboring oxygen atom on the zinc oxide trimer.

There are two vertical states 1 and 2 for ZnO trimer adsorbed on graphene. Hydrolysis of water on ZnO trimer in the vertical 1 state of graphene $C_{30}(ZnO)_3$ does not proceed beyond the first water molecule when the hydrated structures effortlessly reorganize to the final stable hydrolyzed structures $C_{30}O_3ZnO_2(OH)_2$ with negative energies (-167kcal/mol in the singlet and -30.4 kcal/mole in the triplet state)and curve crossing of the singlet and triplet states as displayed in Figure 10 and Table 7. In contrast to this, successive hydration and hydrolysis of two water molecules in the vertical state 2 of the zinc oxide trimer on graphene as shown in the figure 11 and table 8 occurs readily with low activation energies for hydrolysis 0,9 and 1.2 kcal/mol for the first hydrolysis and 26.3 and 2.7 kcal/mol respectively for the

second in the triplet and singlet states, without curve crossing and the energy gap between triplet and singlet states is reduced from -45.5kcal/mol in the initial to -31 kcal /mol in the final hydrolyzed product.
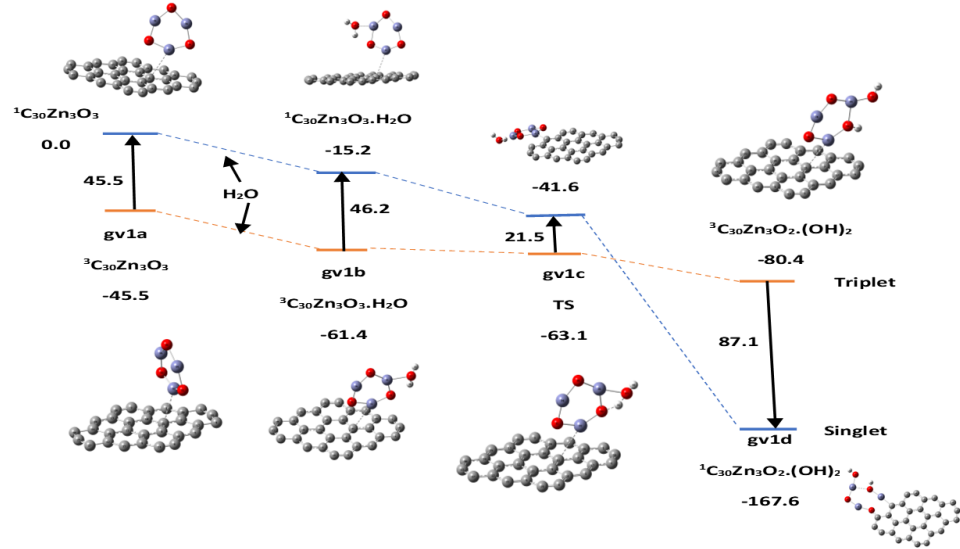
Figure 10: Hydrolysis pathway of one water molecule on $(ZnO)_3$ deposited on graphene:vertical 1

Table 7: Graphene [C_{30}] vertical1-Relative energies in kcal/mol of the adsorption and hydrolysis of the first water molecule in singlet and triplet states shown in Figure 10. The temperature is 298K.

	$\mathbf{Zn_3O_3}$	$\mathbf{Zn_3O_3.H_2O}$	**TS**	$\mathbf{Zn_3O_2(OH)_2}$
	gv1a	gv1b	gv1c	gv1d
E	0.0(S)	-15.2	-41.6	-167.6
	-45.5(T)	-61.4	-63.1	-80.4
$E_{abs,reorg}$		-15.5(S)	-26.4(S)	
		-15.9(T)	-1.7(T)	
Freq			-42.3(S)	
			-883.3(T)	
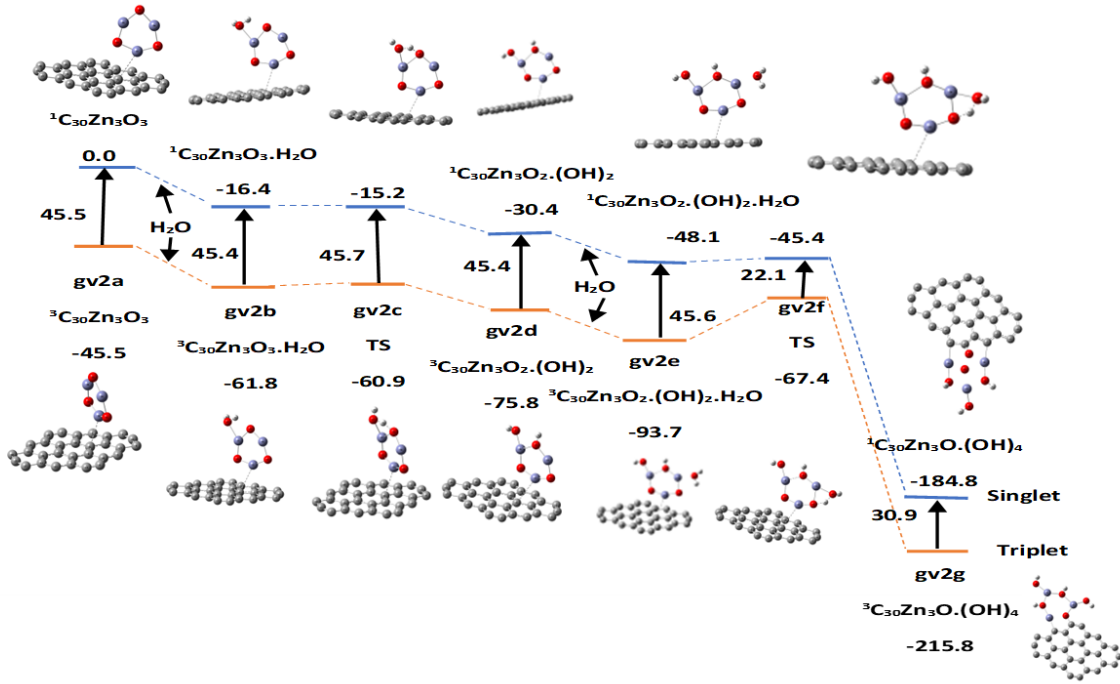
Figure 11: Hydrolysis pathway of one water molecule adorbed on $(ZnO)_3$ deposited on graphene:vertical 2

Table 8: Graphene [C_{30}] vertical2-Relative energies in kcal/mol of the adsorption and hydrolysis of the first water molecule in singlet and triplet states shown in Figure 11. The temperature is 298K.

	Zn_3O_3	$Zn_3O_3.H_2O$	TS	$Zn_3O_2(OH)_2$	$Zn_3O_2(OH)_2.H_2O$	TS	$Zn_3O(OH)_4$
	gv2a	gv2b	gv2c	gv2d	gv2e	gv2f	gv2g
E	0.0(S)	-16.4	-15.2	-30.4	-48.1	-45.4	-184.8
	-45.5(T)	-61.8	-60.9	-75.8	-93.7	-67.4	-215.8
$E_{abs,act}$		-16.4	1.2(S)		-17.7	2.7	
		-16.3	0.9(T)		-17.9	26.3	
Freq			-913.8(S)			-1059.4	
			-910.7(T)			-1064.7	

The trend of low activation energies for the first and second hydrolysis of water molecules continues for the G01 to G05 models even along different pathways although the structural intermediates may not be the same. This is illustrated in Figures 12 to 20 for the mechanistic pathways and the corresponding Tables 9 to 12 for the associated energies for hydration and hydrolysis. The real bottlenecks begin with the next few steps of water splitting.

22
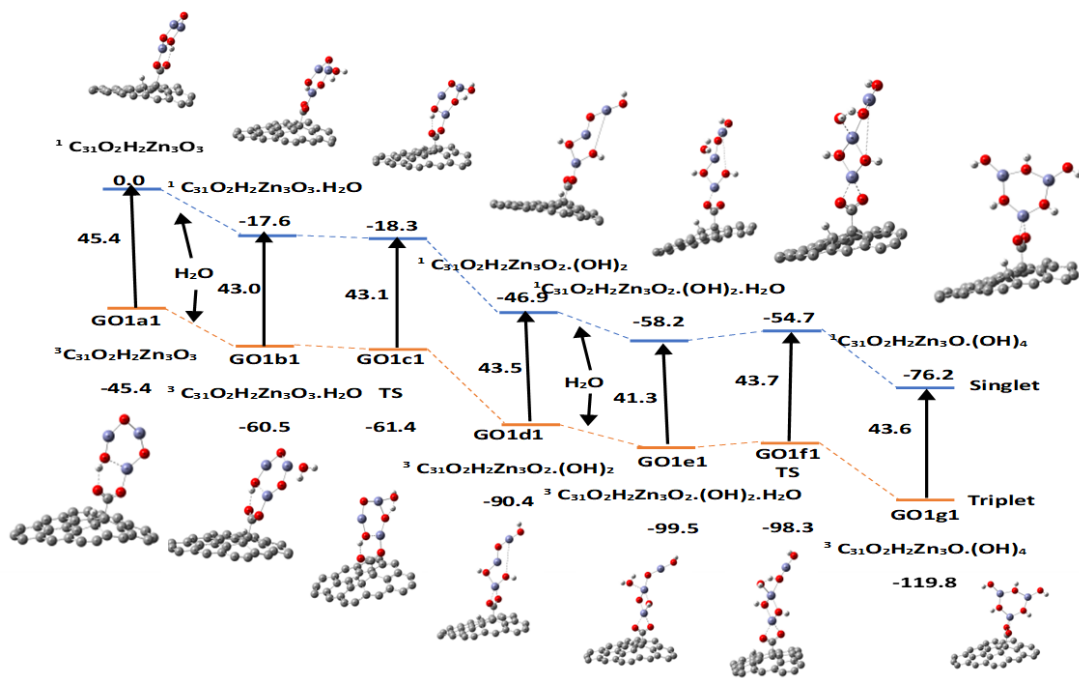
Figure 12: Potential energy surface (PES) of the hydration and hydrolysis of two water molecules on GO1:pathway 1, using B3LYP/DGDZVP2 level of theory.Relative Energies in kcal/mol. The temperature is 298K.
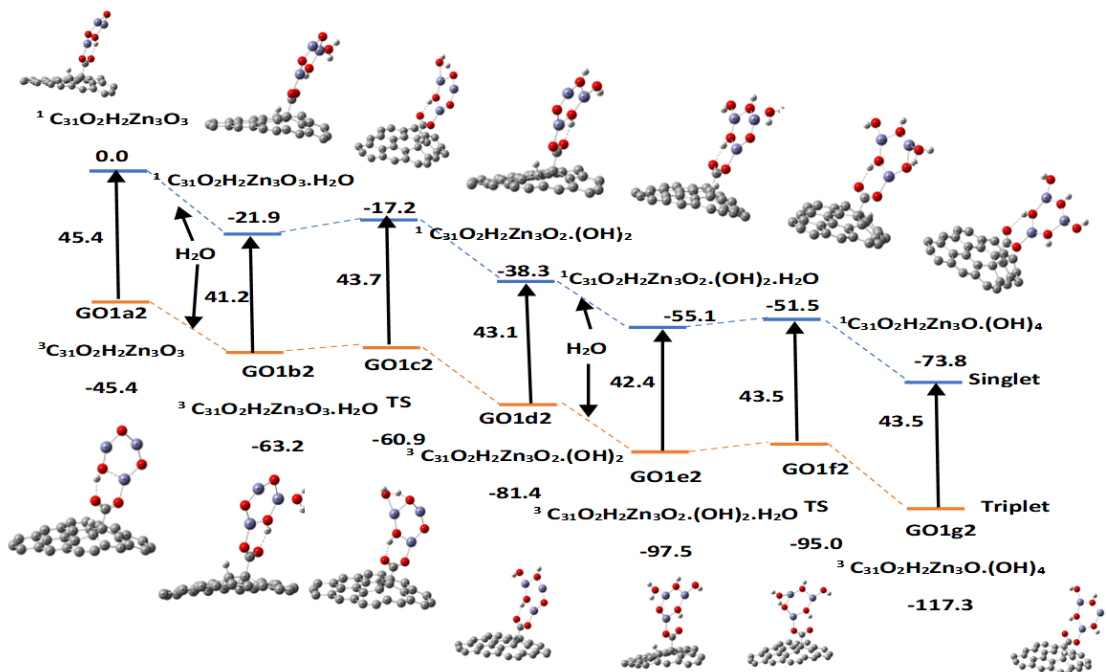
Figure 13: Potential energy surface (PES) of the hydration and hydrolysis of two water molecules on GO1:pathway 2, using B3LYP/DGDZVP2 level of theory.Relative Energies in kcal/mol. The temperature is 298K.

Table 9: Relative energies in kcal/mol of the adsorption and hydrolysis of the first and second water molecules on GO1 [$C_{31}O_2H_2$] prior to water splitting on singlet and triplet states shown in Figure 12 and 13. The temperature is 298K.

	$GO1Zn_3O_3$	$C_{31}O_2H_2Zn_3O_3.H_2O$	TS	$GO1Zn_3O_2(OH)_2$	$GO1Zn_3O_2(OH)_2.H_2O$	TS	$GO1Zn_3O(OH)_4$
PW1	GO1a1	GO1b1	GO1c1	GO1d1	GO1e1	GO1f1	GO1g1
E	0.0(S)	-17.6	-18.3	-46.9	-58.2	-54.7	-76.2
	-45.4(T)	-60.5	-61.4	-90.4	-99.5	-98.3	-119.8
$E_{abs,act}$		-17.6	-0.7(S)		-11.3	3.5	
		-15.1	-0.9(T)		-9.1	1.2	
Freq			-702.7(S)			-958.1	
			-696.8(T)			-955.3	
PW2	GO1a2	GO1b2	GO1c2	GO1d2	GO1e2	GO1f2	GO1g2
E	0.0(S)	-21.9	-17.2	-38.3	-55.1	-51.5	-73.8
	-45.4(T)	-63.2	-60.9	-81.4	-97.5	-95.0	-117.3
$E_{abs,act}$		-21.9	4.7(S)		-16.8	3.6	
		-17.8	2.3(T)		-16.1	2.5	
Freq			-1051.4(S)			-1089.9	
			-1042.7(T)			-1086.2	
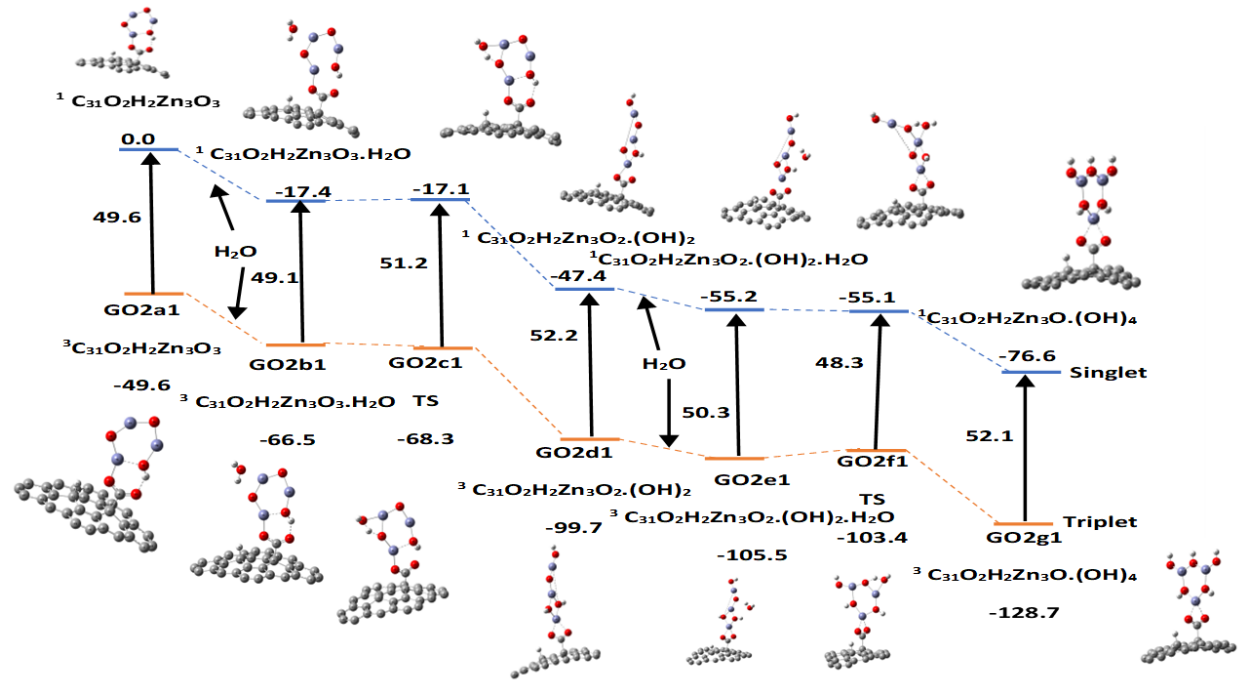
Figure 14: Potential energy surface (PES) of the hydration and hydrolysis of water molecules on GO2:pathway 1, a using B3LYP/DGDZVP2 level of theory.Relative Energies in kcal/mol.
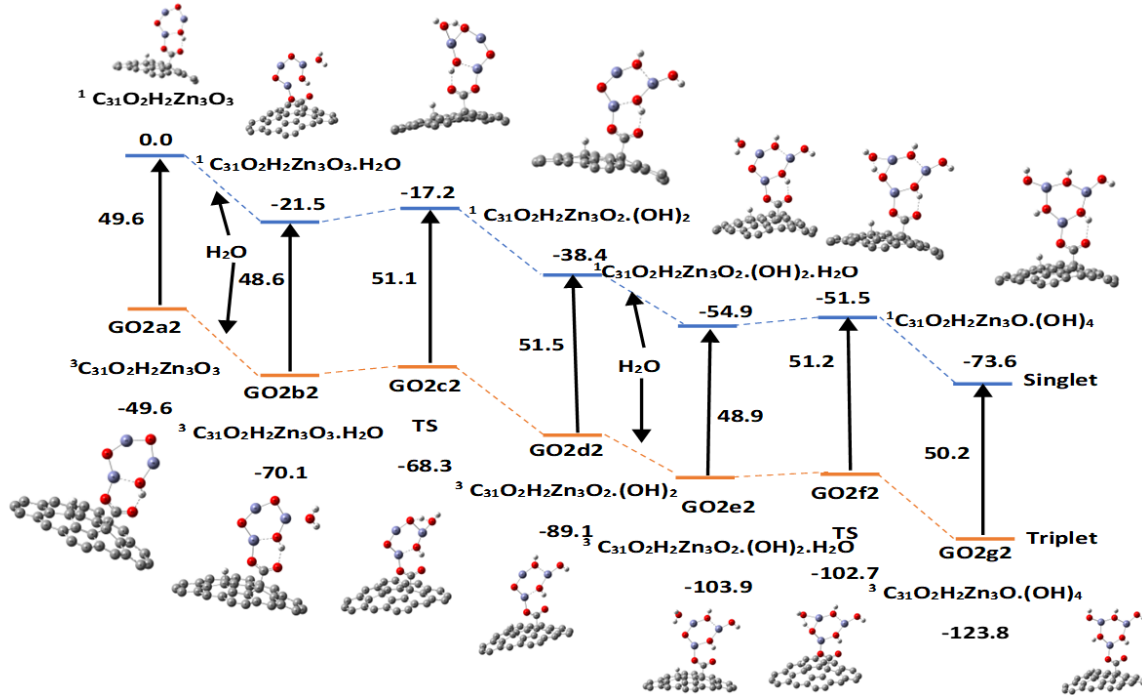
Figure 15: Potential energy surface (PES) of the hydration and hydrolysis of two water molecules on GO2[$C_{31}O_2H_2$]: pathway 2, using B3LYP/DGDZVP2 level of theory. Relative Energies in kcal/mol.

Table 10: GO2-Relative energies in kcal/mol of the adsorption and hydrolysis of the first and second water molecules prior to water splitting on singlet and triplet states shown in Figure 14 and 15. The temperature is 298K.

	GO2Zn_3O_3	$C_{31}O_2H_2Zn_3O_3.H_2O$	TS	GO2$Zn_3O_2(OH)_2$	GO2$Zn_3O_2(OH)_2.H_2O$	TS	GO2$Zn_3O(OH)_4$
PW1	GO2a1	GO2b1	GO2c1	GO2d1	GO2e1	GO2f1	GO2g1
E	0.0(S)	-17.4	-17.1	-47.4	-55.2	-55.1	-76.6
	-49.6(T)	-66.5	-68.3	-99.7	-105.5	-103.4	-128.7
$E_{abs,act}$		-17.4	0.3(S)		-7.8	0.1	
		-16.9	-1.8(T)		-5.8	2.1	
Freq			-687.1(S)			-956.3	
			-668.9(T)			-1051.3	
PW2	GO2a2	GO2b2	GO2c2	GO2d2	GO2e2	GO2f2	GO2g2
E	0.0(S)	-21.5	-17.2	-38.4	-54.9	-51.5	-73.6
	-49.6(T)	-70.1	-68.3	-89.1	-103.9	-102.7	-123.8
$E_{abs,act}$		-21.5	4.3(S)		-16.5	3.4	
		-20.5	1.8(T)		-14.8	1.2	
Freq			-1035.8(S)			-1086.9	
			-1019.9(T)			-1073.5	
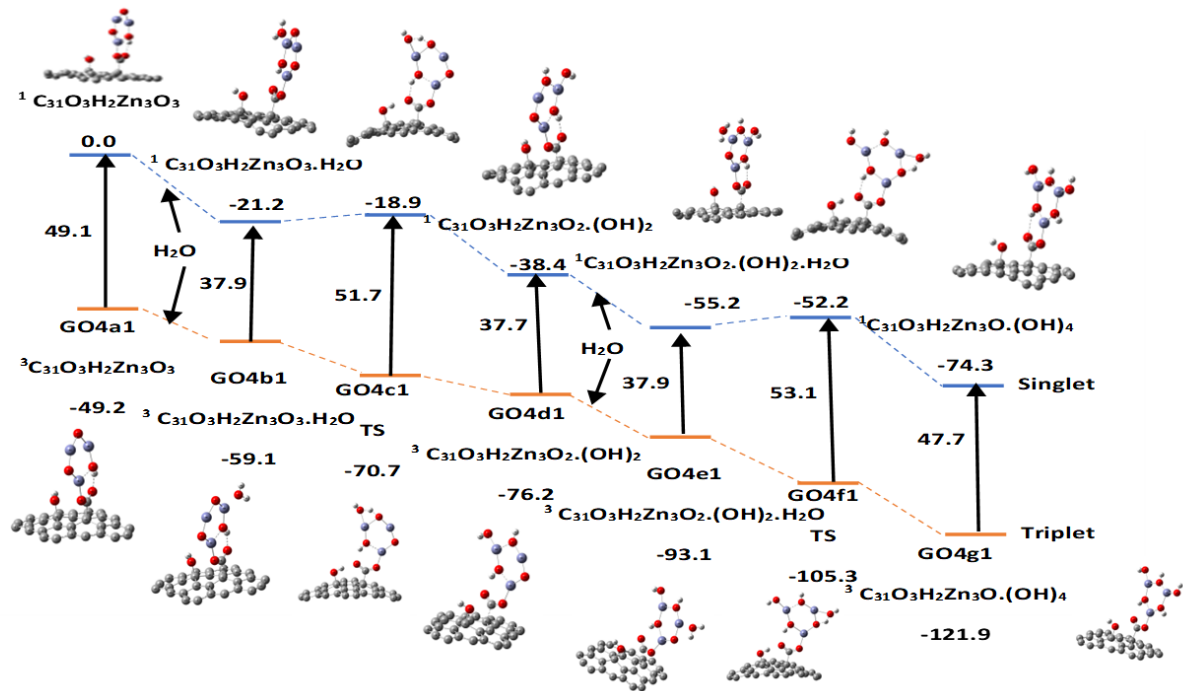
Figure 16: Potential energy surface (PES) of the hydration and hydrolysis of two water molecules on GO4:pathway 1, using B3LYP/DGDZVP2 level of theory.Relative Energies in kcal/mol.
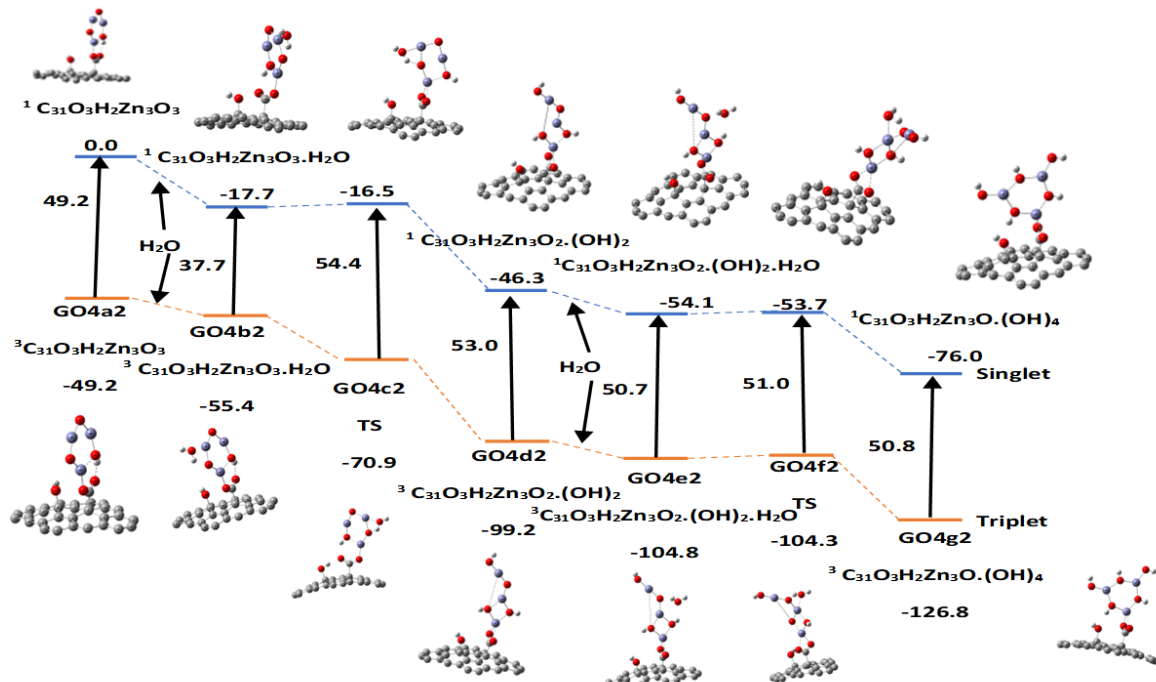
Figure 17: Potential energy surface (PES) of the hydration and hydrolysis of two water molecules on GO4:pathway 2, using B3LYP/DGDZVP2 level of theory.Relative Energies in kcal/mol.

Table 11: GO4: $C_{31}O_3H_2$-Relative energies in kcal/mol of the adsorption and hydrolysis of the first and second water molecules prior to water splitting on singlet and triplet states shown in Figure 16 and 17. The temperature is 298K.

	$GO4Zn_3O_3$	$GO4Zn_3O_3.H_2O$	TS	$GO4Zn_3O_2(OH)_2$	$GO4Zn_3O_2(OH)_2.H_2O$	TS	$GO4Zn_3O(OH)_4$
PW1	GO4a1	GO4b1	GO4c1	GO4d1	GO4e1	GO4f1	GO4g1
E	0.0(S)	-21.2	-18.9	-38.4	-55.2	-52.2	-74.3
	-49.2(T)	-59.1	-70.7	-76.2	-93.1	-105.3	-121.9
$E_{abs,act}$		-21.2	2.3(S)		-16.8	3.0	
		-9.9	-11.6(T)		-16.9	-12.2	
Freq			-1056.3(S)			-1104.6	
			-1037.1(T)			-1079.4	
PW2	GO4a2	GO4b2	GO4c2	GO4d2	GO4e2	GO4f2	GO4g2
E	0.0(S)	-17.7	-16.5	-46.3	-54.1	-53.7	-76.0
	-49.2(T)	-55.4	-70.9	-99.2	-104.8	-104.3	-126.8
$E_{abs,act}$		-17.7	1.2(S)		-7.8	0.4	
		-6.2	-15.5(T)		-5.6	0.5	
Freq			-99.1(S)			-953.9	
			-659.9(T)			-946.4	
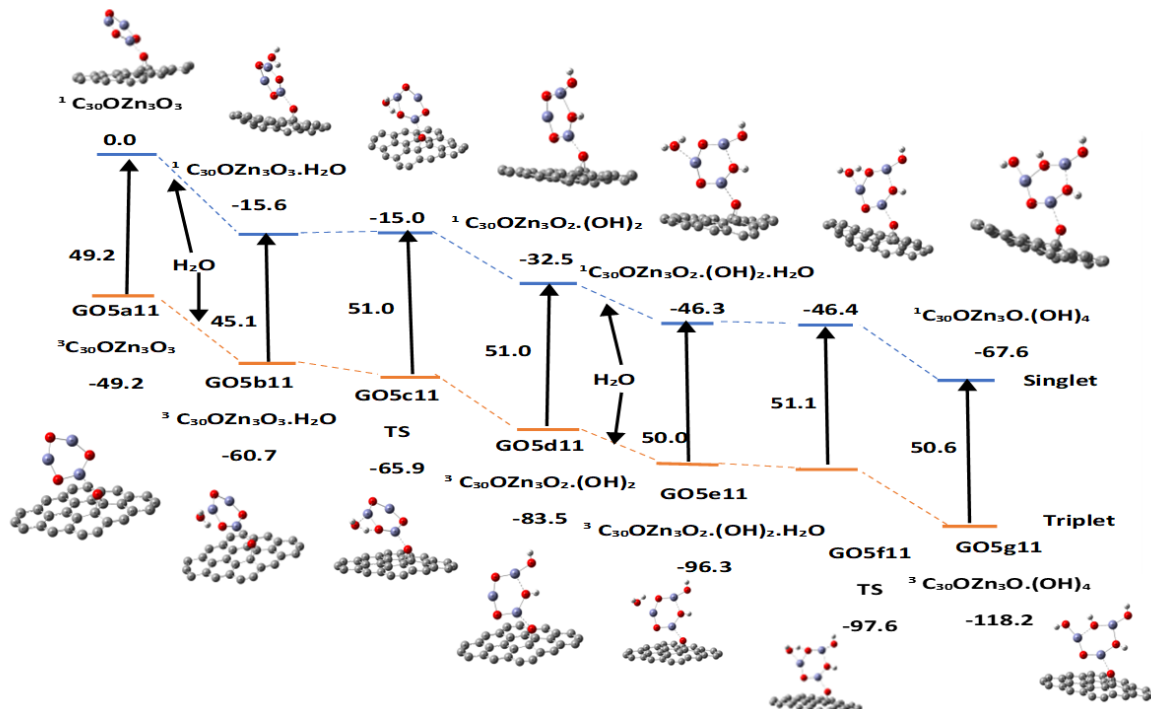
Figure 18: Potential energy surface (PES) of the hydration and hydrolysis of two water molecules on GO5:pathway 1a, using B3LYP/DGDZVP2 level of theory.Relative Energies in kcal/mol.
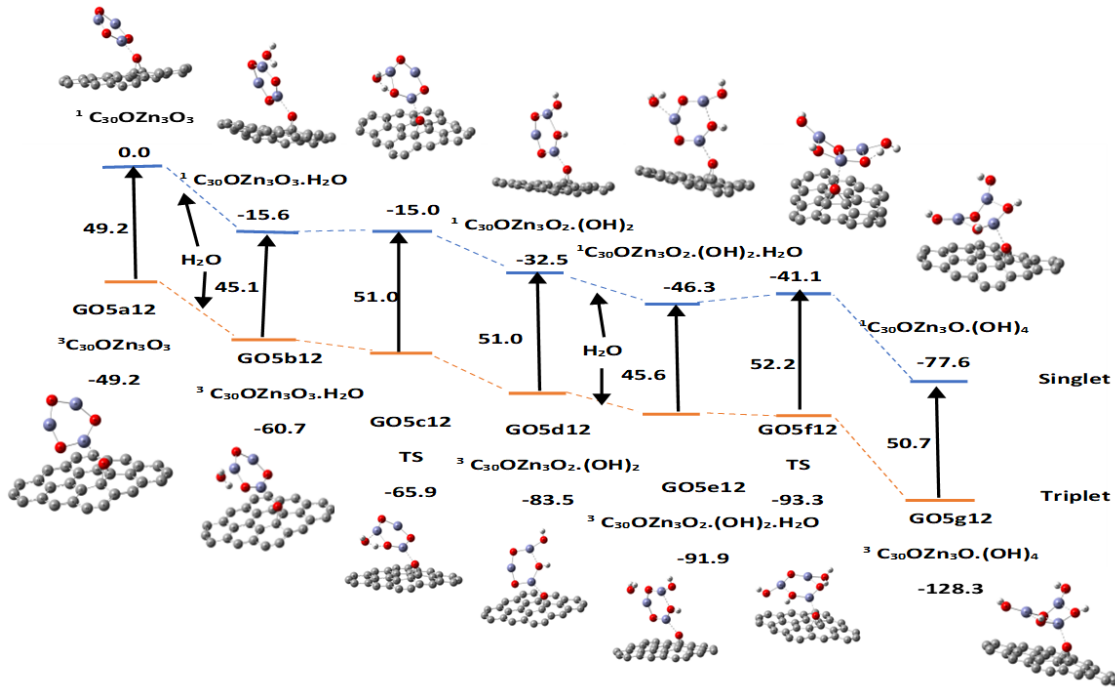
Figure 19: Potential energy surface (PES) of the hydration and hydrolysis of two water molecules on GO5:pathway 1b, using B3LYP/DGDZVP2 level of theory.Relative Energies in kcal/mol.
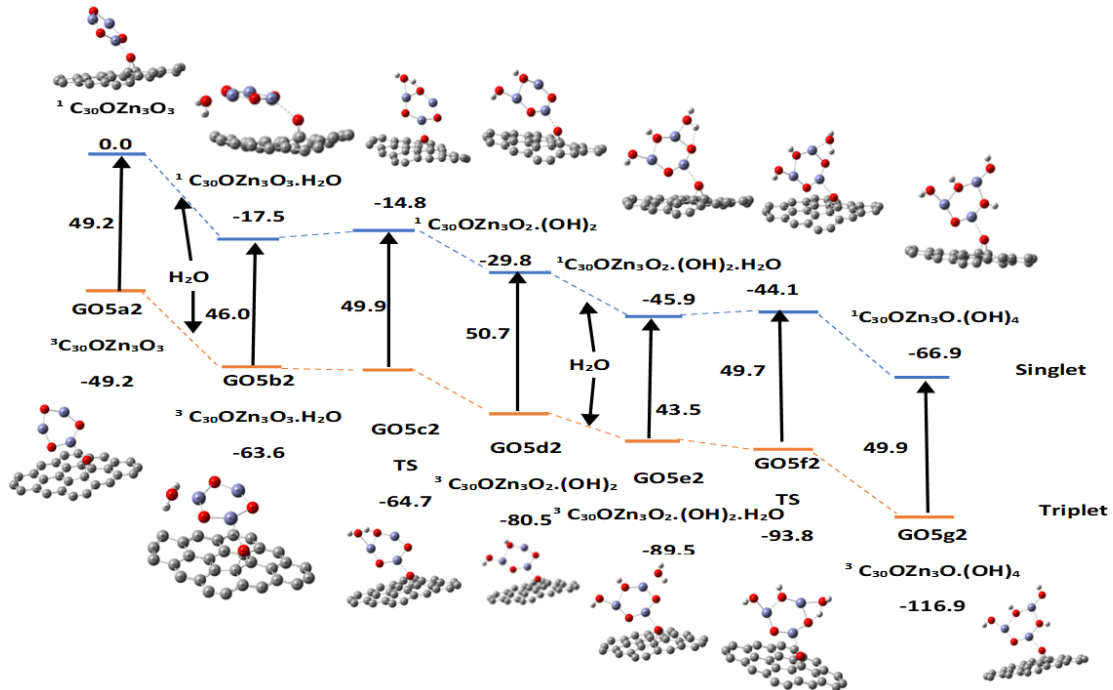
Figure 20: Potential energy surface (PES) of the hydration and hydrolysis of two water molecules on GO5:pathway 2, using B3LYP/DGDZVP2 level of theory.Relative Energies in kcal/mol.

Table 12: GO5[$C_{30}O$]-Relative energies in kcal/mol of the formation and release of the first hydrogen molecule during water splitting shown in Figure 18, 19 and 20. The temperature is 298K.

	GO5Zn$_3$O$_3$	GO5Zn$_3$O$_3$.H$_2$O	TS	GO5Zn$_3$O$_2$(OH)$_2$	GO5Zn$_3$O$_2$(OH)$_2$.H$_2$O	TS	GO5Zn$_3$O(OH)$_4$
PW1a	GO5a11	GO5b11	GO5c11	GO5d11	GO5e11	GO5f11	GO5g11
E	0.0(S)	-15.6	-15.0	-32.5	-46.3	-46.4	-67.6
	-49.2(T)	-60.7	-65.9	-83.5	-96.3	-97.6	-118.2
E$_{abs,act}$		-15.6	0.6(S)		-13.8	-0.1	
		-11.5	-5.2(T)		-12.8	-1.3	
Freq			-934.9(S)			-678.2	
			-843.8(T)			-786.7	
PW1b	GO5a12	GO5b12	GO5c12	GO5d12	GO5e12	GO5f12	GO5g12
E	0.0(S)	-15.6	-15.0	-32.5	-46.3	-41.1	-77.6
	-49.2(T)	-60.7	-65.9	-83.5	-91.9	-93.3	-128.3
E$_{abs,act}$		-15.6	0.6(S)		-13.8	5.2	
		-11.5	-5.2(T)		-8.4	1.4	
Freq			-934.9(S)			-456.1	
			-843.8(T)			-975.1	
PW2	GO5a2	GO5b2	GO5c2	GO5d2	GO5e2	GO5f2	GO5g2
E	0.0(S)	-17.5	-14.8	-29.8	-45.9	-44.1	-66.9
	-49.2(T)	-63.6	-64.7	-80.5	-89.5	-93.8	-116.9
E$_{abs,act}$		-17.5	2.7(S)		-16.1	1.8	
		-14.4	-1.1(T)		-9.0	-4.3	
Freq			-887.2(S)			-994.3	
			-856.0(T)			-1008.1	

Table 13 shows the relative energies and energy changes of hydration and hydrolysis reaction of bare $(ZnO)_3$ and $(ZnO)_3$ on graphene and GO systems with two water molecules. According to that, graphene itself would not be able to use as a substrate for water spitting. The overall energy change for hydrolysis on graphene is -167.76 kcal/mol the vertical state 1 is unlikely as the rate-determining because of their low activation energies. The reaction pathways for hydrolysis reaction on the vertical 1 graphene system were worked only on the triplet state. The hydrolysis reaction of $(ZnO)_3$ on the vertical 2 graphene system was successful on both states with one water molecule but not with the second water molecule. This can occur due to transferring the hydrophobic property from the graphene sheet to the $(ZnO)_3$ on the singlet state.

Table 13: Relative Energies and energy changes of Hydration and hydrolysis of $(ZnO)_3$ on different systems, $S(0)$ = singlet $S(1)$ = triplet
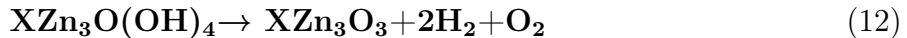
system		E_{bare}	$E_{hydrol1}$	$DE_{hydrol1}$	$E_{hydrol2}$	$DE_{hydrol2}$	
$(ZnO)_3$							
	Path a S(1)	57.5	11.3	-42.3	-14.9	-72.4	Table4 [46]
	S(0)	0.0	-31.2	-31.2	-78.3	-78.3	
							Table4 [46]
	Pathb1	57.5	11.3	-42.3	-14.7	-72.2	
		0.0	-31.2	-31.2	-79.9	-79.7	
	Pathb2	57.5	11.3		-14.7	-72.4	Table4 [46]
		0.0	-31.2		-78.3	-78.3	
GV1	V1 Singlet S(0)	0	-167.6	-167.6	NA	NA	Table 7
	Tripet S(1)	-45.5	-80.5	-34.9	NA	NA	
GV2	V2(S0)	0.0	-30.4	-30.4	-184.8	-184.8	Table 8
	S(1)	-45.5	-75.8	-30.3	-215.8	-170.3	
GO1	P1 S(0)	0.0	-46.9	-46.9	-76.2	-76.2	Table 9
	S(1)	-45.4	38.3	-45	-119.8	-74.4	
	P2 S(0)	0.0	-38.3	-38.3	-73.8	-73.8	
	S(1)	-45.4	-81.4	-35.9	117.3	-71.9	
GO2	P1 S(0)	0.0	-47.4	-47.4	-76.6	-76.6	Table 10
	S(1)	-49.6	-99.7	-50.1	-128.7	-79.1	
	P2 S(0)	0.0	-38.4	-38.4	-73.6	-73.6	
	S(1)	-49.6	-89.1	-39.5	-123.8	-74.2	
GO4							
	P1 (S0)	0.0	-38.4	-38.4	-74.3	-74.3	Table 11
	S(1)	-49.2	-76.2	-26.2	-121.9	-72.7	
	P2 S(0)	0.0	-46.3	-46.3	-76	-76	
	S(1)	-49.2	-99.2	-50	-126.8	-77.6	
GO5							
	P1a S(0)	0.0	-32.5	-32.5	-67.6	-67.6	Table 12
	S(1)	-49.2	-83.5	-50.1	-118.2	-69	
	P1b S(0)	0.0	-46.3	-46.3	77.6	-77.6	Table 12
	S(1)	-49.2	-99.2	-50	-128.3	-79.1	
	P2 S(0)	0.0	-29.8	-29.8	-66.9	-66.9	Table 12
	S(1)	-49.2	-80.5	-31.3	-116.9	-67.7	

$(ZnO)_3$ with GO models shows similar hydrolysis reaction pathways as in bare $(ZnO)_3$. GO1, GO2, and GO4 models have two different hydrolysis reaction pathways whereas GO5 has 3 different hydrolysis reaction pathways. All the transition states in both singlet and triplet states are calculated using the Berny algorithm. The transition states have only one negative frequency as shown in the relative tables. The low activation energy barriers interpret the lower impact of the hydrolysis reaction pathway for the rate-determining step of the water-splitting reaction.

Water Splitting Results

GO1 model

In this section, we consider the final steps in the mechanism and energetics of water splitting on the GO1 model from the hydrolyzed product to get H_2, O_2 and cluster model as the catalysts as shown in eq12 where X denoted the GO model (here it is the GO1 model, $C_{31}O_2H_2$).

$$\textbf{XZn}_3\textbf{O(OH)}_4 \rightarrow \textbf{XZn}_3\textbf{O}_3 + \textbf{2H}_2 + \textbf{O}_2 \qquad (12)$$

This reaction is highly endothermic with an enthalpy change of 116 kcal/mol at 298K. The intermediate steps in the reaction determine the overall rate of water splitting in the GO1 model, by comparing it with our previous study of water splitting using the bare $(ZnO)_3$ nanocatalyst. Figure 21 and 22 show the intermediate steps involved in the evolution of the first hydrogen molecule; the corresponding potential energy values are summarized in Table 14 and 15. Clearly, the rate-determining step is the rearrangement of the intermediate. All transition states have negative frequency values as shown in the table 14 and 15.

The energy change for the rearrangement is $\approx$94.2 kcal/mol in the triplet and singlet states and the corresponding activation energies are $\approx$ 112.5 kcal/mol showing that the rearrangement is more likely the rate-determining step as already shown for the bare $(ZnO)_3$ nan-

Table 14: Relative energies in kcal/mol of the formation and release of the first hydrogen molecule during water splitting on GO1 model shown in Figure 21. The temperature is 298K.

	$GO1Zn_3O(OH)_4$	TS	$HZn_3O_2(OH)_3$	TS	$Zn_3O_3(OH)_2.H_2$	$Zn_3O_3(OH)_2$	TS
Pathway 1	GO1g1	GO1h1	GO1i1	GO1j1	GO1k1	GO1l1	GO1m1
E	-76.2	36.3	18.3	54.1	37.1	36.1	NA
	-119.8	-7.4	-25.6	11.1	-6.3	-7.3	NA
$E_{ad,act}$	-76.2	112.5(S)		35.8			
	-74.4	112.4(T)		36.7			
Freq		-684.1		-1237.3			
		-687.5		-1235.1			

ocluster for which the rearrangement energies of 53.5 and 76. kcal/mol in the triplet and singlet states and corresponding activation energies of 82.8 and 120.8 kcal/mol in the triplet and singlet states respectively. The rearrangement energies though smaller in the activation energies of the bare ZnO trimer are slightly larger (120 vs 112kcal/mol) in our calculations for the bare ZnO trimer nanocatalyst.
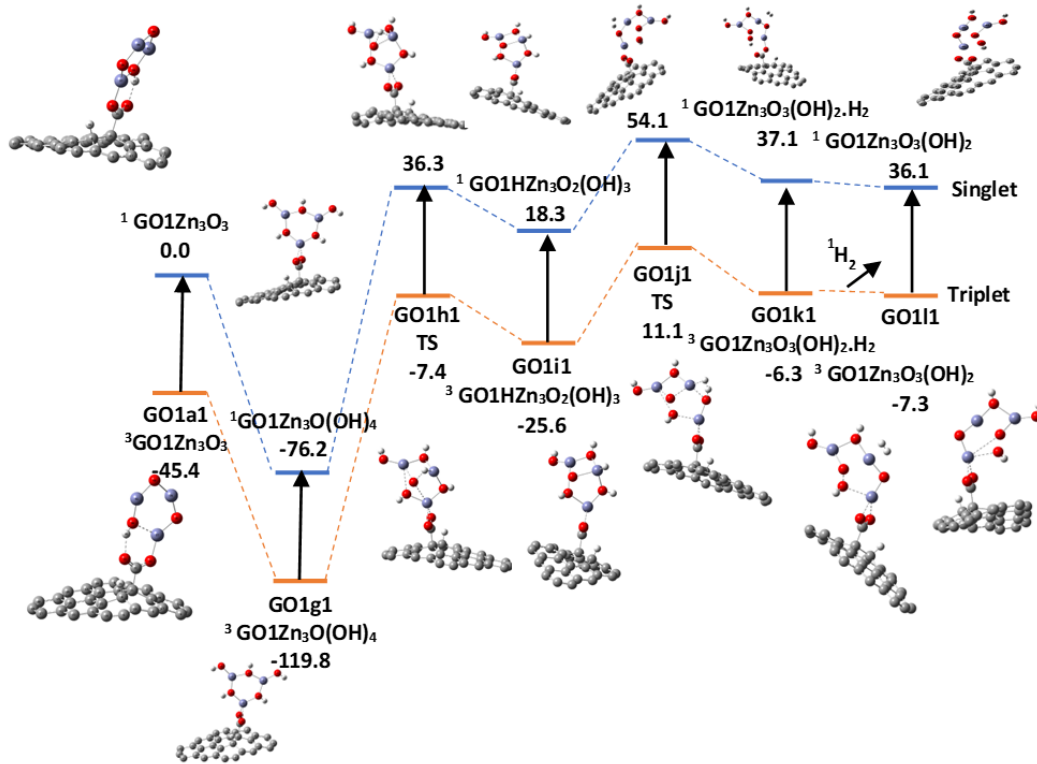
Figure 21: Water splitting reaction on $GO1[C_{31}O_2H_2]$ towards the first H_2 desorption:pathway 1.

After the first H_2 desorption occurred, the remaining 'H' atoms in the structure l (GO1l1 in

the figure 21 in both singlet and triplet states) are rearranged in a favorable way to make an H-H bond to form the second H_2 molecule. Hence the structure m and n from the reaction pathway can be eliminated.
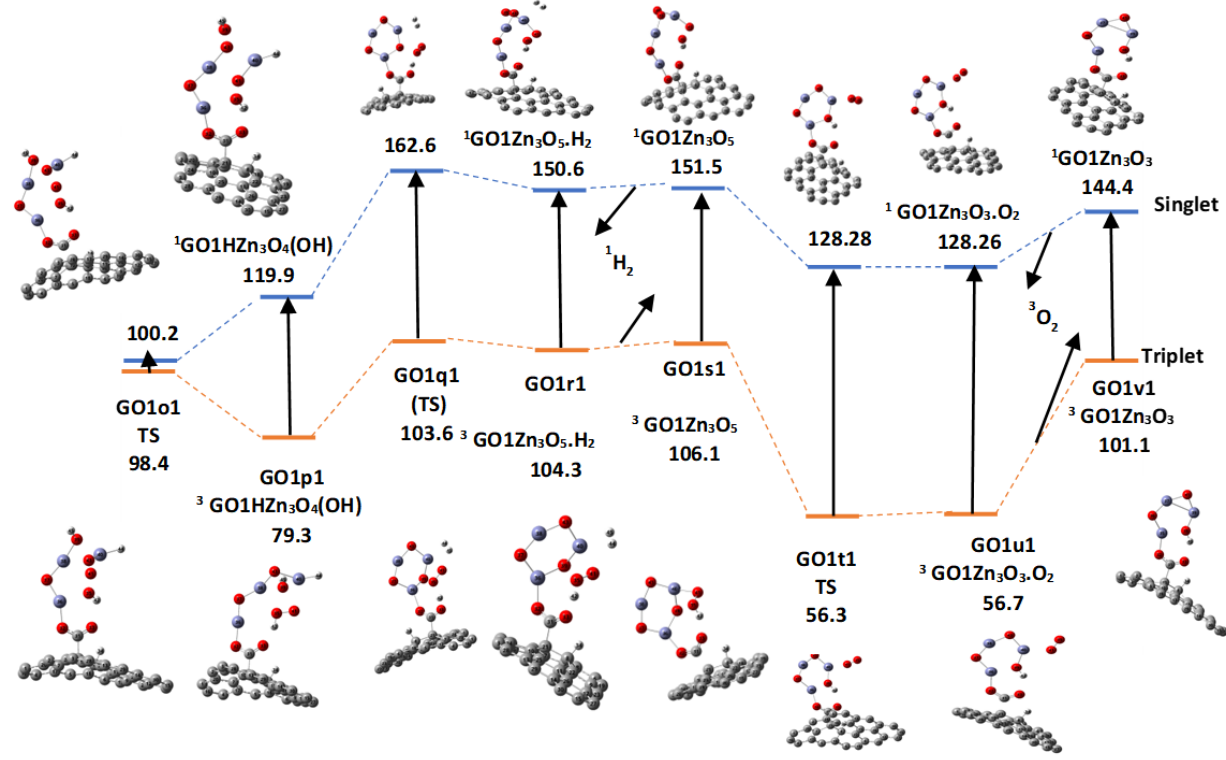
Figure 22: Water splitting on GO1[$C_{31}O_2H_2$] towards the second H_2 and O_2 desorption:pathway 1.

Table 15: Relative energies in kcal/mol of the formation and release of the first hydrogen molecule during water splitting on GO1 model shown in Figure 22. The temperature is 298K.

	GO1Zn$_3$O$_3$(OH)$_2$	TS	GO1HZn$_3$O$_4$(OH)	TS	GO1Zn$_3$O$_5$.H$_2$	GO1Zn$_3$O$_5$	TS	GO1Zn$_3$O$_3$.O$_2$	GO1Zn$_3$O$_3$
Pathway 1	GO1n1	GO1o1	GO1p1	GO1q1	GO1r1	GO1s1	GO1t1	GO1u1	GO1v1
E	NA	100.2	119.9	162.6	150.6	151.5	128.28	128.26	144.4
	NA	98.4	79.3	103.5	104.3	106.1	56.3	56.7	101.1
E$_{ad,act}$	NA	64.1(S)		42.7			-23.3		
	NA	105.7(T)		24.3			-49.8		
Freq		-65.2		-27.5			-29.8		
		-43.6		-1104.7			-26.7		

Figure 23 compares the water splitting reaction on bare $(ZnO)_3$ and GO1-$(ZnO)_3$ system. The singlet and triplet states of bare $(ZnO)_3$ and the GO1-$(ZnO)_3$ systems are represented in blue, orange, grey, and yellow color lines respectively. The triplet state of GO1-$(ZnO)_3$ has
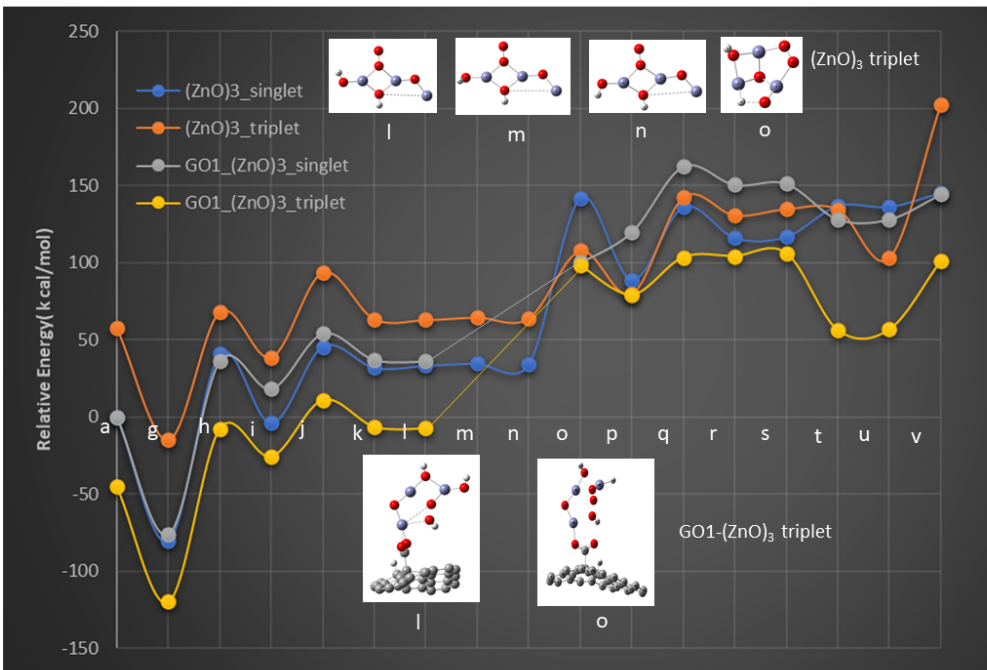
Figure 23: Schematic comparison of Water splitting reaction on bare $(ZnO)_3$ and $GO1[C_{31}O_2H_2]$ towards the H_2 and O_2 desorption:pathway 1.

the lowest energy. Both singlet and triplet states in both systems have similar arrangements during the first H_2 desorption. $GO1$-$(ZnO)_3$ models skip two steps (structure m and n) in the second H_2 desorption. The singlet-triplet states crossed during the O_2 desorption on bare $(ZnO)_3$ but not in the $GO1$-$(ZnO)_3$ system.

Conclusion

Graphene and graphene-based metal oxides are considered suitable substrates for metal oxide photocatalysts for water-splitting reactions. In this work, we selected $(ZnO)_3$ nanocluster as the metal oxide catalyst after careful consideration. The π conjugation structure of GO shows great electron mobility and may enhance the photocatalytic performance of ZnO by increasing the electron-hole separation. The hydration and hydrolysis reaction $(ZnO)_3$ nanocluster absorbed on graphene was studied in both singlet and triplet states using B3LYP/DGDZVP2 exchange functionals and basis sets. The hydration and hydrolysis reaction on GO models

were also studied on both singlet and triplet states using the same combination of exchange functional and basis sets. GO models 1, 2, and 4 have two different reaction pathways for the hydrolysis reaction, and GO model 5 has three different hydrolysis reaction pathways as the Zn atom only binds with the O atom in the epoxy group. The triplet state of GO1-$(ZnO)_3$ has the lowest relative energy compared to the bare $(ZnO)_3$. The splitting reaction pathway with GO1-$(ZnO)_3$ skips "m" and "n" steps as described as the geometry of "l" is already in a favorable conformation to split water and produce H_2 molecules.

Acknowledgement

Supporting Information Available

The Supporting Information (SI) document is available for free of charge.

References

(1) Fujishima, A.; Honda, K. Electrochemical Photolysis of Water at a Semiconductor Electrode. *Nature* **1972**, *238*, 37–38, Bandiera_abtest: a Cg_type: Nature Research Journals Number: 5358 Primary_atype: Research Publisher: Nature Publishing Group.

(2) Razek, S. A.; Popeil, M. R.; Wangoh, L.; Rana, J.; Suwandaratne, N.; Andrews, J. L.; Watson, D. F.; Banerjee, S.; Piper, L. F. J. Designing catalysts for water splitting based on electronic structure considerations. *Electronic Structure* **2020**, *2*, 023001, Publisher: IOP Publishing.

(3) Eidsvåg, H.; Bentouba, S.; Vajeeston, P.; Yohi, S.; Velauthapillai, D. TiO2 as a Photocatalyst for Water Splitting—An Experimental and Theoretical Review. *Molecules* **2021**, *26*, 1687.

(4) Li, D.; Liu, H.; Feng, L. A Review on Advanced FeNi-Based Catalysts for Water Splitting Reaction. *Energy & Fuels* **2020**, *34*, 13491–13522, Publisher: American Chemical Society.

(5) Galińska, A.; Walendziewski, J. Photocatalytic Water Splitting over PtTiO2 in the Presence of Sacrificial Reagents. *Energy & Fuels* **2005**, *19*, 1143–1147, Publisher: American Chemical Society.

(6) Fang, Z.; Dixon, D. A. Computational Study of H2 and O2 Production from Water Splitting by Small (MO2)n Clusters (M = Ti, Zr, Hf). *The Journal of Physical Chemistry A* **2013**, *117*, 3539–3555, Publisher: American Chemical Society.

(7) Du, X.; Skachko, I.; Barker, A.; Andrei, E. Y. Approaching ballistic transport in suspended graphene. *Nature Nanotechnology* **2008**, *3*, 491–495, Bandiera_abtest: a Cg_type: Nature Research Journals Number: 8 Primary_atype: Research Publisher: Nature Publishing Group.

(8) An, X.; Yu, J. C. Graphene-based photocatalytic composites. *RSC Advances* **2011**, *1*, 1426–1434, Publisher: The Royal Society of Chemistry.

(9) Xiang, Q.; Yu, J.; Jaroniec, M. Graphene-based semiconductor photocatalysts. *Chemical Society Reviews* **2012**, *41*, 782–796, Publisher: The Royal Society of Chemistry.

(10) Zhang, N.; Zhang, Y.; Xu, Y.-J. Recent progress on graphene-based photocatalysts: current status and future perspectives. *Nanoscale* **2012**, *4*, 5792–5813, Publisher: The Royal Society of Chemistry.

(11) Han, L.; Wang, P.; Dong, S. Progress in graphene-based photoactive nanocomposites as a promising class of photocatalyst. *Nanoscale* **2012**, *4*, 5814–5825, Publisher: The Royal Society of Chemistry.

(12) Zhu, Z.; Su, M.; Ma, L.; Ma, L.; Liu, D.; Wang, Z. Preparation of graphene oxide–silver nanoparticle nanohybrids with highly antibacterial capability. *Talanta* **2013**, *117*, 449–455.

(13) Tang, J.; Chen, Q.; Xu, L.; Zhang, S.; Feng, L.; Cheng, L.; Xu, H.; Liu, Z.; Peng, R. Graphene Oxide–Silver Nanocomposite As a Highly Effective Antibacterial Agent with Species-Specific Mechanisms. *ACS Applied Materials & Interfaces* **2013**, *5*, 3867–3874, Publisher: American Chemical Society.

(14) Cobos, M.; De-La-Pinta, I.; Quindós, G.; Fernández, M. J.; Fernández, M. D. Synthesis, Physical, Mechanical and Antibacterial Properties of Nanocomposites Based on Poly(vinyl alcohol)/Graphene Oxide–Silver Nanoparticles. *Polymers* **2020**, *12*, 723, Number: 3 Publisher: Multidisciplinary Digital Publishing Institute.

(15) Zang, Z.; Zeng, X.; Wang, M.; Hu, W.; Liu, C.; Tang, X. Tunable photoluminescence of water-soluble AgInZnS–graphene oxide (GO) nanocomposites and their application in-vivo bioimaging. *Sensors and Actuators B: Chemical* **2017**, *252*, 1179–1186.

(16) Chen, D.; Feng, H.; Li, J. Graphene Oxide: Preparation, Functionalization, and Electrochemical Applications. *Chemical Reviews* **2012**, *112*, 6027–6053, Publisher: American Chemical Society.

(17) Standley, B.; Mendez, A.; Schmidgall, E.; Bockrath, M. Graphene-graphite oxide field-effect transistors. *Nano Letters* **2012**, *12*, 1165–1169.

(18) Dideikin, A. T.; Vul', A. Y. Graphene Oxide and Derivatives: The Place in Graphene Family. *Frontiers in Physics* **2019**, *0*, Publisher: Frontiers.

(19) Georgakilas, V.; Tiwari, J. N.; Kemp, K. C.; Perman, J. A.; Bourlinos, A. B.; Kim, K. S.; Zboril, R. Noncovalent Functionalization of Graphene and Graphene Oxide for Energy Materials, Biosensing, Catalytic, and Biomedical Applications. *Chemical Reviews* **2016**, *116*, 5464–5519, Publisher: American Chemical Society.

(20) Khan, M.; Tahir, M. N.; Adil, S. F.; Khan, H. U.; Siddiqui, M. R. H.; Al-warthan, A. A.; Tremel, W. Graphene based metal and metal oxide nanocomposites: synthesis, properties and their applications. *Journal of Materials Chemistry A* **2015**, *3*, 18753–18808, Publisher: The Royal Society of Chemistry.

(21) Parnianchi, F.; Nazari, M.; Maleki, J.; Mohebi, M. Combination of graphene and graphene oxide with metal and metal oxide nanoparticles in fabrication of electrochemical enzymatic biosensors. *International Nano Letters* **2018**, *8*, 229–239.

(22) Zhang, H.; Wang, X.; Li, N.; Xia, J.; Meng, Q.; Ding, J.; Lu, J. Synthesis and characterization of TiO2/graphene oxide nanocomposites for photoreduction of heavy metal ions in reverse osmosis concentrate. *RSC Advances* **2018**, *8*, 34241–34251, Publisher: The Royal Society of Chemistry.

(23) Martins, P.; Ferreira, C.; Silva, A.; Magalhães, B.; Alves, M.; Pereira, L.; Marques, P.; Melle-Franco, M.; Lanceros-Méndez, S. TiO 2 /graphene and TiO 2 /graphene oxide nanocomposites for photocatalytic applications: A computer modeling and experimental study. *Composites Part B: Engineering* **2018**, *145*, 39–46.

(24) Tayel, A.; Ramadan, A. R.; El Seoud, O. A. Titanium Dioxide/Graphene and Titanium Dioxide/Graphene Oxide Nanocomposites: Synthesis, Characterization and Photocatalytic Applications for Water Decontamination. *Catalysts* **2018**, *8*, 491, Number: 11 Publisher: Multidisciplinary Digital Publishing Institute.

(25) Do, H. H.; Nguyen, D. L. T.; Nguyen, X. C.; Le, T.-H.; Nguyen, T. P.; Trinh, Q. T.; Ahn, S. H.; Vo, D.-V. N.; Kim, S. Y.; Le, Q. V. Recent progress in TiO2-based pho-

tocatalysts for hydrogen evolution reaction: A review. *Arabian Journal of Chemistry* **2020**, *13*, 3653–3671.

(26) Yeh, T.-F.; Cihlář, J.; Chang, C.-Y.; Cheng, C.; Teng, H. Roles of graphene oxide in photocatalytic water splitting. *Materials Today* **2013**, *16*, 78–84.

(27) Chen, C.; Cai, W.; Long, M.; Zhou, B.; Wu, Y.; Wu, D.; Feng, Y. Synthesis of Visible-Light Responsive Graphene Oxide/TiO2 Composites with p/n Heterojunction. *ACS Nano* **2010**, *4*, 6425–6432, Publisher: American Chemical Society.

(28) Ahn, B. D.; Kang, H. S.; Kim, J. H.; Kim, G. H.; Chang, H. W.; Lee, S. Y. Synthesis and analysis of Ag-doped ZnO. *Journal of Applied Physics* **2006**, *100*, 093701, Publisher: American Institute of PhysicsAIP.

(29) Kang, H. S.; Kang, J. S.; Kim, J. W.; Lee, S. Y. Annealing effect on the property of ultraviolet and green emissions of ZnO thin films. *Journal of Applied Physics* **2004**, *95*, 1246, Publisher: American Institute of PhysicsAIP.

(30) Look, D. C.; Reynolds, D. C.; Sizelove, J. R.; Jones, R. L.; Litton, C. W.; Cantwell, G.; Harsch, W. C. Electrical properties of bulk ZnO. *Solid State Communications* **1998**, *105*, 399–401.

(31) Wenas, W. W.; Yamada, A.; Takahashi, K.; Yoshino, M.; Konagai, M. Electrical and optical properties of boron-doped ZnO thin films for solar cells grown by metalorganic chemical vapor deposition. *Journal of Applied Physics* **1991**, *70*, 7119–7123, Publisher: American Institute of Physics.

(32) Wang, Z. Nanobelts, Nanowires, and Nanodiskettes of Semiconducting Oxides—From Materials to Nanodevices. *Advanced Materials* **2003**, *15*, 432–436, _eprint: https://onlinelibrary.wiley.com/doi/pdf/10.1002/adma.200390100.

(33) Inoue, T.; Fujishima, A.; Konishi, S.; Honda, K. Photoelectrocatalytic reduction of carbon dioxide in aqueous suspensions of semiconductor powders. *Nature* **1979**, *277*, 637–638, Bandiera_abtest: a Cg_type: Nature Research Journals Number: 5698 Primary_atype: Research Publisher: Nature Publishing Group.

(34) Watanabe, M. Photosynthesis of methanol and methane from CO2 and H2O molecules on a ZnO surface. *Surface Science Letters* **1992**, *279*, L236–L242.

(35) Gouvêa, D.; Ushakov, S. V.; Navrotsky, A. Energetics of CO2 and H2O Adsorption on Zinc Oxide. *Langmuir* **2014**, *30*, 9091–9097, Publisher: American Chemical Society.

(36) Hernández, S.; Hidalgo, D.; Sacco, A.; Chiodoni, A.; Lamberti, A.; Cauda, V.; Tresso, E.; Saracco, G. Comparison of photocatalytic and transport properties of TiO2 and ZnO nanostructures for solar-driven water splitting. *Physical Chemistry Chemical Physics* **2015**, *17*, 7775–7786, Publisher: The Royal Society of Chemistry.

(37) Min, Y.; Zhang, K.; Chen, L.; Chen, Y.; Zhang, Y. Ionic liquid assisting synthesis of ZnO/graphene heterostructure photocatalysts with tunable photoresponse properties. *Diamond and Related Materials* **2012**, *26*, 32–38.

(38) Xu, T.; Zhang, L.; Cheng, H.; Zhu, Y. Significantly enhanced photocatalytic performance of ZnO via graphene hybridization and the mechanism study. *Applied Catalysis B: Environmental* **2011**, *101*, 382–387.

(39) Akhavan, O. Graphene Nanomesh by ZnO Nanorod Photocatalysts. *ACS Nano* **2010**, *4*, 4174–4180, Publisher: American Chemical Society.

(40) Wang, J.; Gao, Z.; Li, Z.; Wang, B.; Yan, Y.; Liu, Q.; Mann, T.; Zhang, M.; Jiang, Z. Green synthesis of graphene nanosheets/ZnO composites and electrochemical properties. *Journal of Solid State Chemistry* **2011**, *184*, 1421–1427.

(41) Meyer, B.; Marx, D.; Dulub, O.; Diebold, U.; Kunat, M.; Langenberg, D.; Wöll, C. Partial Dissociation of Water Leads to Stable Superstructures on the Surface of Zinc Oxide. *Angewandte Chemie International Edition* **2004**, *43*, 6641–6645, _eprint: https://onlinelibrary.wiley.com/doi/pdf/10.1002/anie.200461696.

(42) Tocci, G.; Michaelides, A. Solvent-Induced Proton Hopping at a Water–Oxide Interface. *The Journal of Physical Chemistry Letters* **2014**, *5*, 474–480, Publisher: American Chemical Society.

(43) Quaranta, V.; Behler, J.; Hellström, M. Structure and Dynamics of the Liquid–Water/Zinc-Oxide Interface from Machine Learning Potential Simulations. *The Journal of Physical Chemistry C* **2019**, *123*, 1293–1304, Publisher: American Chemical Society.

(44) Quaranta, V.; Hellström, M.; Behler, J. Proton-Transfer Mechanisms at the Water–ZnO Interface: The Role of Presolvation. *The Journal of Physical Chemistry Letters* **2017**, *8*, 1476–1483, Publisher: American Chemical Society.

(45) Raymand, D.; van Duin, A. C.; Goddard, W. A.; Hermansson, K.; Spångberg, D. Hydroxylation Structure and Proton Transfer Reactivity at the Zinc OxideWater Interface. *The Journal of Physical Chemistry C* **2011**, *115*, 8573–8579, Publisher: American Chemical Society.

(46) Perera, D. C.; Rasaiah, J. C. Exchange Functionals and Basis Sets for Density Functional Theory Studies of Water Splitting on Selected ZnO Nanocluster Catalysts. *ACS Omega* **2022**, *7*, 12556–12569, Publisher: American Chemical Society.

(47) Huang, L.; Gubbins, K. E. Ammonia Dissociation on Graphene Oxide: An Ab Initio Density Functional Theory Calculation. *Zeitschrift für Physikalische Chemie* **2015**, *229*, 1211–1223, Publisher: Oldenbourg Wissenschaftsverlag.

(48) http://www.chemistry4.me/Gaussian/G09W/help/pbctut2.htm.

(49) Frisch, M. J. et al. Gaussian~16 Revision C.01. 2016; Gaussian Inc. Wallingford CT.

(50) Dennington, R.; Keith, T. A.; Millam, J. M. GaussView Version 6. 2019; Semichem Inc. Shawnee Mission KS.